Title

Exact Many-Body Solution of the Periodic-Cluster t-t'-J Model for Cubic Systems: Ground-State Properties

Authors

Freericks, J.K.
Falicov, L.M.

Publication Date

1990-05-01

LBL-28995
Preprint

Lawrence Berkeley Laboratory

UNIVERSITY OF CALIFORNIA

Materials & Chemical Sciences Division

Submitted to Physical Review B

Exact Many-Body Solution of the Periodic-Cluster t-t′-J Model for Cubic Systems: Ground-State Properties

J.K. Freericks and L.M. Falicov

May 1990

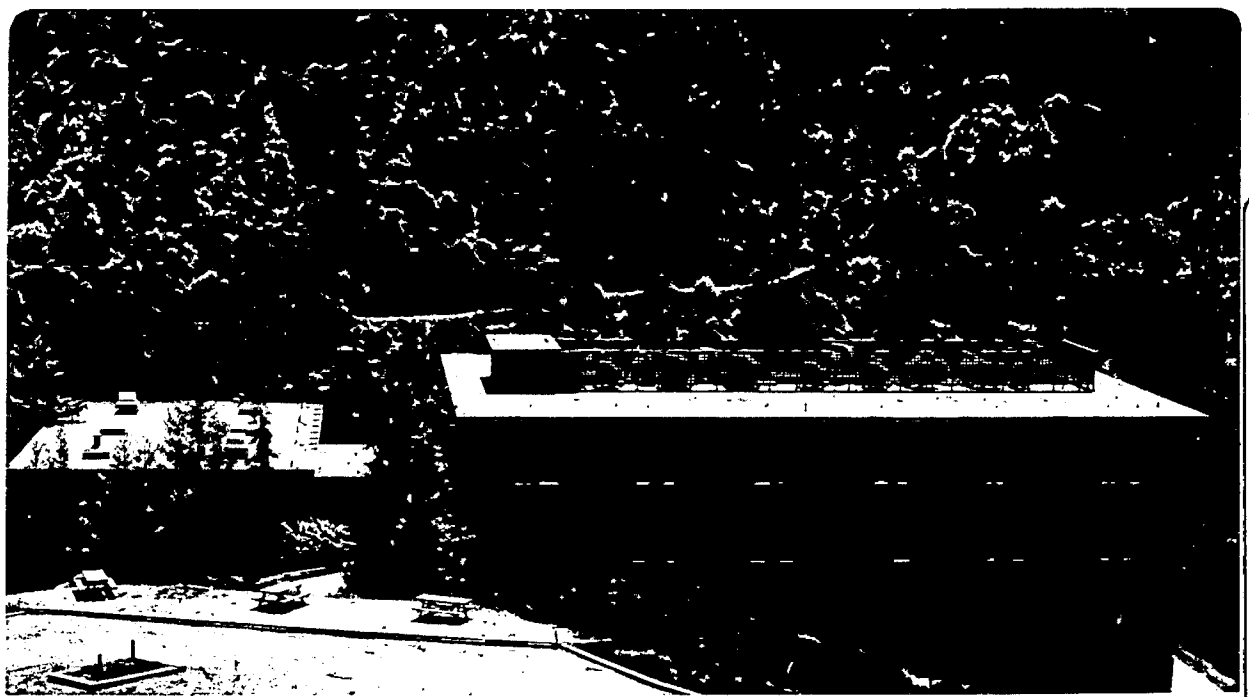

Prepared for the U.S. Department of Energy under Contract Number DE-AC03-76SF00098.

DISCLAIMER

LBL-28995

EXACT MANY-BODY SOLUTION OF THE PERIODIC-CLUSTER t-t'-J MODEL FOR CUBIC SYSTEMS: GROUND-STATE PROPERTIES*

J. K. Freericks and L. M. Falicov

Department of Physics
University of California, Berkeley, CA 94720

and

Materials and Chemical Sciences Division,
Lawrence Berkeley Laboratory,
Berkeley, CA 94720

May 1990

---

*This work was supported by the Director, Office of Energy Research, Office of Basic Energy Sciences, Materials Sciences Division of the U. S. Department of Energy under Contract No. DE-AC03-76SF00098.

Exact Many-Body Solution of the Periodic-Cluster t–t′–J Model for Cubic Systems: Ground-State Properties

J. K. Freericks and L. M. Falicov

Department of Physics,
University of California,
Berkeley, CA 94720,

and

Materials and Chemical Sciences Division,
Lawrence Berkeley Laboratory,
Berkeley, CA 94720.

ABSTRACT

The t–t'–J model (strongly interacting limit of a particular Hubbard model) is solved exactly on small clusters of eight sites with periodic boundary conditions for the simple, body-centered, and face-centered cubic lattices and for the two-dimensional square lattice. The symmetry, k-vector and spin of the ground state are studied as functions of crystalline environment, interaction strength, and electron concentration. Phase diagrams are presented for stable solutions, and regions of parameter space that exhibit ferromagnetism and heavy-fermionic behavior are identified.

May 4, 1990

1990 PACS number(s): 71.10.+x; 71.28.+d; 75.10.Lp.

Exact Many-Body Solution of the Periodic-Cluster t–t′–J Model for Cubic Systems: Ground-State Properties

J. K. Freericks and L. M. Falicov

Department of Physics,
University of California,
Berkeley, CA 94720,

and

Materials and Chemical Sciences Division,
Lawrence Berkeley Laboratory,
Berkeley, CA 94720.

I. Introduction

Strong electron correlation is responsible for long-range-order magnetic materials,[1] heavy fermion (HF) behavior,[2,3] and high-temperature superconductivity.[4,5] The $t-t'-J$ model is the simplest model of an interacting electronic system that mimics the strong correlation effects present in these materials. In ferromagnetic and HF systems this model describes the mutual interaction and effective electron transfer of the narrow $d-$ and f-band electrons while in the high-temperature superconductors it approximates the hole-hole interaction and hole hopping in the CuO_2 planes.

The $t-t'-J$ model is defined on a lattice with one spherically symmetric orbital per site by the following Hamiltonian:

$$H = H_{1NN} + H_{2NN} + H_{int} \quad , \tag{1}$$

where[6]

$$H_{1NN} = -\ t \sum_{\substack{i,j;\sigma \\ <i,j> = 1NN}} (1-n_{i-\sigma})\, c^{\dagger}_{i\sigma}\, c_{j\sigma}\, (1-n_{j-\sigma}) \quad , \tag{2a}$$

$$H_{2NN} = -\ t' \sum_{\substack{i,j;\sigma \\ <i,j> = 2NN}} (1-n_{i-\sigma})\, c^{\dagger}_{i\sigma}\, c_{j\sigma}\, (1-n_{j-\sigma}) \quad , \tag{2b}$$

$$H_{int} = J \sum_{\substack{i,j \\ <i,j> = 1NN}} \mathbf{S}_i \cdot \mathbf{S}_j \quad . \tag{2c}$$

In these equations $c_{i\sigma}^{\dagger}$ ($c_{i\sigma}$) are creation (destruction) operators for an electron in the orbital at site i with z-component of spin σ, $n_{i\sigma} = c_{i\sigma}^{\dagger} c_{i\sigma}$ is the corresponding number operator, and $\mathbf{S}_i$ is the vector spin of an electron at site i. The terms in H include a band "hopping" interaction between conduction states on nearest-neighbor sites (2a) and next-nearest-neighbor sites (2b) and an antiferromagnetic nearest-neighbor Heisenberg superexchange interaction term (2c) with exchange integral $2J$. The hopping terms contain projection operators that prevent double occupation of any orbital.

This Hamiltonian has two interpretations: it is an electronic system with indirect exchange interactions and a "super" Pauli principle that forbids electrons of like *or* unlike spin from occupying the same spatial site; or it is an approximation to the $U \rightarrow \infty$ limit of the single-band Hubbard[7] model

$$H_{Hubb} = - t \sum_{\substack{i,j;\sigma \\ <i,j> = 1NN}} c_{i\sigma}^{\dagger} c_{j\sigma} - t' \sum_{\substack{i,j;\sigma \\ <i,j> = 2NN}} c_{i\sigma}^{\dagger} c_{j\sigma} + U \sum_i n_{i\downarrow} n_{i\uparrow} \quad . \tag{3}$$

Anderson[8] first showed the equivalence of the half-filled band Hubbard model at large interaction strength to the Heisenberg model. His proof was based upon second-order perturbation theory: At half-filling and infinite U each lattice site is singly occupied and all spin states are degenerate. When U is made finite, the lowest order correction to the energy comes from virtual processes where an electron hops to its nearest neighbor (if the spins are antiparallel) and then hops back. The energy gain for such a fluctuation is $\simeq t^2/U$ since doubly occupied states have energy $\simeq U$. This hopping creates the Heisenberg superexchange interaction term to lowest order in t/U. Away from half-filling, the electrons can hop from occupied to empty sites and additional fluctuations that involve three sites (an electron hops to a neighboring occupied site and then hops to a third unoccupied site) are present. Schrieffer and Wolff[9] found a canonical transformation to the single-occupied sector of a related model that was valid

for arbitrary fillings. This technique was applied to the Hubbard model to first order,[10] and recently to arbitrary order.[11] Since the t–t'–J Hamiltonian (1) only involves the nearest-neighbor superexchange interaction, it approximates the canonically transformed Hubbard Hamiltonian (3) in the limit of large U when $J = 2t^2/U$ and when any terms of order $O(t^2/U^2)$ or $O(t'^2/tU)$ and any three-site hopping terms in the transformed Hubbard Hamiltonian are neglected. This approximation is exact at half-filling for $t' = 0$ but becomes increasingly less accurate with hole concentration away from half-filling.

A few rigorous results are known about the t–t'–J model:

(a) At half-filling it reduces to a Heisenberg model whose ground state[12] is a nondegenerate singlet on bipartite lattices and possibly ferrimagnetic for other cases. Lieb[13] recently extended this analysis to the Hubbard model with finite U.

(b) The case of one hole in a half-filled band at $J = 0$ ($U = \infty$) is known to be ferromagnetic[14] (Nagaoka's theorem) when $t' \leq 0$ for the simple cubic (sc), body-centered cubic (bcc), and the square (sq) lattices for all t and for the face-centered cubic (fcc) when $t < 0$.

(c) The one-dimensional t–t'–J model with free boundary conditions and an even number of electrons has a spin-singlet ground state.[15]

(d) The one-dimensional Hubbard model has been solved exactly with the Bethe ansatz for arbitrary fillings by Lieb and Wu[16] which yields solutions[17,18] to the t–t'–J model at $t' = 0$ and $J = 0$ ($U = \infty$).

(e) The Bethe ansatz has also been applied[19] to the one-dimensional t–t'–J model with $t = J$ and $t' = 0$.

Aside from these theorems little else is known rigorously about the solutions of this many-body problem. The standard approach is to apply variational, perturbative, or mean-field approximations to such interacting models. We choose an alternate

method which is exact, but subject to finite-size effects. It is called the small-cluster approach.[20]

The small-cluster approach begins with the periodic crystal approximation:[21] A bulk crystal of M atoms is modeled by a lattice of M sites with periodic boundary conditions (PBC). Bloch's theorem then labels the electron many-body wavefunctions by one of M k-vectors of the first Brillouin zone. The standard approach takes the thermodynamic limit ($M \rightarrow \infty$), which replaces the finite grid in reciprocal space by a continuum that spans the Brillouin zone. Electron correlation effects are then treated in an approximate fashion. The small-cluster approach takes the opposite limit: The number of sites is chosen to be a small number ($M = 8$) restricting the sampling in momentum space to a few high-symmetry points. However, the interacting electronic system is solved *exactly* taking into account all electron correlation effects. The one-electron band structure of these two methods is identical when sampled at the common points in reciprocal space. The relationship of the many-body solutions (at equal electron concentration) for the macroscopic crystal and the small cluster is much more complicated due to uncontrolled finite-size effects in the latter. Nevertheless, the small-cluster approach does provide an alternate means of rigorously studying the many-body problem and (possibly) extrapolating these results to macroscopic crystals.

The small-cluster approach was proposed independently for the Hubbard model by Harris and Lange[10] and Falicov and Harris[22] with the exact solution of a two-site cluster. Subsequent work concentrated on the ground–state[23] and thermodynamic[24] properties of the one-dimensional half-filled band Hubbard model on four- and six-site clusters.

The first truly three-dimensional case to be investigated was the eight-site *sc* cluster. Ground-state properties at infinite[25] and finite[26] U and thermodynamic[25–27] properties have all been studied. The solution of the four-site square (sq) and tetrahedral (fcc) clusters[28] marked the first time that group theory was used to factorize the

Hamiltonian into block-diagonal form by using basis functions of definite spin that transform according to irreducible representations of the full space group.

Takahashi[29] studied the ground-state spin as a function of electron filling in the infinite U limit of the Hubbard model on a variety of clusters (up to twelve sites). Unfortunately, the use of free boundary conditions (instead of PBC) introduces strong surface effects that complicate extrapolation to the thermodynamic limit. The effect of geometry on the ground state has also been examined[30] for finite U.

The t–t'–J model was solved for 7 electrons in eight-site *fcc* bulk[31] and surface[32] clusters. The bulk calculation illustrates clearly the power of group-theoretical techniques, where a 1024×1024 matrix is diagonalized *in closed form* after being block-diagonalized. Recent work has concentrated on the square lattice at half-filling and with one or two holes.[33] The cluster sizes are large (up to 18 sites) so only the low-lying eigenvalues and eigenvectors were determined.

The small-cluster approach has also been applied to the study of real materials. It is quite successful in describing properties that depend on short-range many-body correlations. These include photoemission in transition metals,[34] alloy formation,[35] surface photoemission[36] in Ni and Co, and surface magnetization[37] in Fe. This technique has also been applied to multi-band versions of the Hubbard model that describes high-temperature superconductivity in the CuO_2 planes.[38]

In this contribution we examine the ground-state symmetry, k-vector, and spin as a function of electron concentration and interaction strength for the t–t'–J model on eight-site clusters for *sc, bcc, fcc,* and *sq* lattices with PBC. In the next section we describe the method of calculation used; in section III we present our results for the ground-state properties, phase diagrams for regions of stability in parameter space, and we identify ferromagnetic ground-state solutions; in section IV we examine low-lying excitations in the many-body spectra to determine regions in parameter space where HF behavior is expected; in the final section we present our conclusions and some

conjectures.

II. Calculational Details

The dimension of the Hamiltonian matrix grows exponentially with the size of the cluster (*e.g.*, an M-site cluster with one orbital per site has dimension $4^M \times 4^M$). This rapid growth restricts the maximum size of the cluster to be on the order of 10 sites. In the strong-interaction regime (*i.e.*, the t–t'–J model), double-occupancy of an orbital is forbidden, reducing the Hilbert space from 4^M to 3^M (for eight-site clusters this corresponds to an order of magnitude simplification from 65536 to 6561). The systematic use of conserved quantities and symmetries of the Hamiltonian provides further simplifications.

The total-number operator $N = \sum_{i,\sigma} n_{i\sigma}$ commutes with the Hamiltonian in Eq. (1) and is a conserved quantity. The Hilbert space with definite electron number N reduces to dimension $2^N M!/N!(M-N)!$ as summarized in Table I for the eight-site cluster. The largest remaining block size is now 1792×1792 for the 5 and 6 electron cases.

The electronic states can be further characterized by their spin and spatial symmetries. Since the total spin, the total z-component of spin, and the total spin raising and lowering operators all commute with the Hamiltonian, the many-body states may be labelled by the total spin S and the total z-component of spin m_S, with every state in a given spin multiplet degenerate in energy. The spatial symmetry is labelled by the irreducible representation of the space group that transforms according to the many-body state. In our case, the space groups are symmorphic, moderately sized finite groups, that are constructed from the point-group operations and the eight translation vectors of the lattice (see the appendix). The grand orthogonality theorem and the matrix element theorem[39–41] (generalized Unsöld theorem) guarantee that the Hamiltonian matrix will be in block-diagonal form, with no mixing between states of

different spin or spatial symmetry, when it is expanded in a symmetrized basis that has definite spin and transforms according to the (1,1) matrix elements of an irreducible representation of the space group. We have written a symmetry-adapted computer algorithm that, given the lattice structure of a small cluster with PBC (see the appendix), the generators[42] of the space group, and the character table[43] of the space group, calculates the (1,1) matrix elements of the irreducible representations (in a fashion similar to Luehrmann[41]). These matrix elements are used to construct projection operators that operate on maximum z-component of spin states ($m_S = S$) to generate symmetrized basis functions of definite spin and spatial symmetry. The Hamiltonian blocks are determined in this symmetrized basis and are checked for completeness within each subspace of definite spin and spatial symmetry. The resultant blocks are diagonalized by the so-called QL algorithm[44] which determines all of the eigenvalues and eigenvectors in the many-body problem. Table II summarizes the reduced block sizes for the four different lattices considered. The application of full spin and space group symmetry reduces the block sizes by another two orders of magnitude which, in turn, reduces the diagonalization time by six orders of magnitude. This symmetry-adapted algorithm was tested for 7 electrons in an eight-site *fcc* cluster and verified the known analytic results[31] for that case.

The effect of geometry on the many-body solutions to the t–t'–J model is studied by solving the model exactly for four different crystalline environments: the *sc*, *bcc*, *fcc*, and *sq* lattices. The eight-site clusters with PBC for these different structures are illustrated in real space and reciprocal space in Figs. 1-4. The PBC will renormalize the parameters in the Hamiltonian (1) when the summations in Eq. (2) are restricted to run over the finite cluster ($1 \le i, j \le 8$). For example, the six nearest-neighbors of an even (odd) site i in the *sc* lattice (see Fig. 1) are *two* each of the odd (even) sites (excluding the site $9-i$), the twelve next-nearest neighbors are *four* each of the remaining even (odd) sites, and the eight third-nearest neighbors are *eight* each of

the site $9-i$. This renormalizes the parameters in the $t-t'-J$ model by $t \rightarrow 2t$, $t' \rightarrow 4t'$, and $J \rightarrow 2J$. Similar analysis for the other crystalline structures is given in Table III.

The small-cluster approach samples the first Brillouin zone at eight k–vectors, which correspond to only three (bcc, fcc) or four (sc, sq) different symmetry stars. As summarized in Table IV, the one-electron energies of the small-cluster Hamiltonian agree precisely with the one-electron band structure of the infinite crystal, when sampled at the common k-vectors. Some of the properties of the many-body states can be understood by the naive picture of occupying these one-electron levels as if the electrons were non-interacting (see below).

The space groups that are relevant for totally symmetric orbitals on each site of the cluster have 48 (sc), 192 (bcc, fcc) or 64 (sq) distinct elements. They are divided into 10 (sc), 14 (bcc), 13 (fcc), and 16 (sq) classes, respectively. The character tables for these space groups are given in the appendix.

The nearest-neighbor hopping matrix element $|t|$ is chosen to be the unit of energy. Three different cases are examined for the next-nearest-neighbor hopping matrix element: $t' > 0$, $t' = 0$, and $t' < 0$. The magnitude of t' is chosen to be 0.5 for the bcc lattice. This sets $|t'| = 0.15$ for the other three lattices, when exponential dependence of the hopping matrix elements on the distance between lattice sites is assumed.

Finally, we note that whenever the lattice is bipartite (sc, bcc, sq) — *i.e.*, it can be separated into two sublattices A and B such that the nearest-neighbor hopping is $A \rightarrow B$ and $B \rightarrow A$ and the next-nearest-neighbor hopping is $A \rightarrow A$ and $B \rightarrow B$ only — then the $t-t'-J$ model has an eigenvalue spectrum that is symmetric[16] in t. This allows us to limit[45] our discussion to $t = 1$ for the sc, bcc, and sq lattices; while we consider both $t = 1$ and $t = -1$ for the fcc lattice.

III. Results: Ground State Symmetry

The k-vector, spatial (small group of k) symmetry, and spin of the many-body ground state are calculated exactly for all electron fillings ($0 \leq N \leq 8$) and for $0.0 \leq J < 1.0$. The symmetry of the ground state is recorded by attaching the spin-multiplicity ($2S+1$) as a superscript to the symbol for the irreducible representation that transforms according to the many-body state (as given in the appendix). The t–t'–J model on small clusters has many accidental degeneracies; that is, degeneracies that are not required by the spin and space-group symmetries of the underlying lattice (see below). Some of these degeneracies are inherent in the model itself,[7,23] while other degeneracies occur due to finite-size effects[46] (permutation symmetries of the small cluster that are not representable as space group symmetries).

The cases of low electron filling ($N \leq 3$) are well-described by occupying the lowest one-electron energy levels (Table IV). These one-electron energy levels have a rich structure. The lowest level is nondegenerate and has Γ_1 symmetry for the *sc*, *bcc*, *fcc* ($t > 0$), and *sq* lattices, while the lowest level for the *fcc* ($t < 0$) lattice is threefold degenerate with X_1 symmetry. The first excited level is threefold (X_1), sixfold (N_1), or fourfold (L_1) degenerate for the *sc*, *bcc*, and *fcc* lattices, respectively. The *sq* lattice does not have a unique first excited level: when the 2*NN* hopping integral vanishes ($t' = 0$) there is an accidental degeneracy of Σ_1 and X_1, creating a sixfold degenerate level; for $t' > 0$ the ordering is Σ_1 (fourfold degenerate) $< X_1$ (two-fold degenerate), and *vice versa* for $t' < 0$.

Since the case of one electron ($N = 1$) contains no many-body effects, the ground state is formed by occupying the lowest one-electron level. The ground state, therefore, has symmetry ${}^2\Gamma_1$ ($d = 2$) for the *sc*, *bcc*, *fcc* ($t > 0$), and *sq* lattices and ${}^2X_1$ ($d = 6$) for the *fcc* ($t < 0$) lattice. A second electron ($N = 2$) is added by placing[15] it in a spin-singlet state in the same level as the first electron. This results in a ${}^1\Gamma_1$ ($d = 1$) symmetry for the ground state of the *sc*, *bcc*, *fcc* ($t > 0$), and *sq* lattices.

The fcc ($t<0$) lattice has ${}^1\Gamma_{12}$ ($d=2$) symmetry for finite J, but has a spin-degenerate ${}^3X_2 \oplus {}^1\Gamma_{12}$ ($d=11$) ground state when $J=0$ (because of the degeneracy of the one-electron levels).

In general, the addition of a third electron ($N=3$) is made by placing it in the first-excited one-electron energy level. This yields a ${}^2X_1$ ($d=6$), ${}^2N_1$ ($d=12$), and ${}^2L_1$ ($d=8$) ground state for the sc, bcc, and fcc ($t>0$) lattices. The sq lattice has a ${}^2\Sigma_1$ ($d=8$), ${}^2X_1 \oplus {}^2\Sigma_1$ ($d=12$), or ${}^2X_1$ ($d=4$) ground state for $t'>0$, $t'=0$, and $t'<0$ respectively. However, many-body effects begin to play a more important role in the three-electron case. There is a level crossing in the sc ground state from ${}^2X_1$ ($d=6$) to ${}^2\Gamma_{12}$ ($d=4$) at $J/t=0.85100$ when $t'<0$. The fcc ($t<0$) case is even more interesting. It is the first example of a ferromagnetic ground state ${}^4\Gamma_1$ ($d=4$) (resulting from the application of Hund's empirical rule[47]) which undergoes a level crossing to a spin-doublet ${}^2X_2$ ($d=6$) at $J/t=0.29972$ ($t'>0$), $J/t=0.23617$ ($t'=0$), or $J/t=0.15045$ ($t'<0$).

Many-body effects become increasingly more important for $N \geq 4$. The ground-state symmetries are recorded in Tables V-VIII for the cases $4 \leq N \leq 7$.

The half-filled band ($N=8$) reduces to the case[8] of a Heisenberg antiferromagnet. The solutions are all spin-singlets, have symmetry ${}^1\Gamma_1$ ($d=1$) for the sc, bcc, and sq lattices, and have ${}^1\Gamma_1 \oplus {}^1\Gamma_{12}$ ($d=3$) symmetry for the fcc lattices.

Our results agree with previous work for the sc lattice,[25–27] the fcc lattice,[31] and the sq lattice.[48] There are a few salient features of these results that deserve comment:

(a) The case of the sq lattice with $t'=0$ is identical to the bcc lattice with $t'=0$ due to a hidden symmetry of the eight-site sq lattice.

(b) There is a large number of ferromagnetic[49] solutions for $J \ll t$. These solutions occur in the sc lattice ($t' \leq 0, N=4$; $t' \leq 0, N=7$), in the bcc lattice ($t' \leq 0, N=7$), in the fcc ($t<0$) lattice (all $t', N=3$; all $t', N=7$), and in the

sq lattice (all t', $N=7$). The ferromagnetic solutions for $N = 7$ are all examples of Nagaoka's theorem[14] for one hole in a half-filled band at $J = 0$.

(c) There is also a large number of ferrimagnetic[50] solutions for $J \ll t$. When $N = 4$, ferrimagnetic solutions occur for all geometries except the *sc* lattice; when $N = 5$, ferrimagnetism occurs in the *sc* and *fcc* ($t > 0$) lattices; and when $N = 7$, it occurs for all lattices except *fcc* ($t > 0$).

(d) Whenever the Heisenberg interaction J is large enough, the ground state is stabilized in the lowest spin configuration ($S = 0$ for N = even, $S = 1/2$ for N = odd). In particular, the case of two holes ($N = 6$) is always a spin-singlet.

(e) Non-minimal-spin solutions undergo "spin-cascade" transitions, passing through each intermediate spin *en route* to minimal spin solutions, as J is increased. The only exceptions are in the *sc* lattice ($t' \leq 0$, $N=4$ and $t' = 0$, $N=7$) which have one level crossing from maximal spin to minimal spin and the *sq* lattice ($t' < 0$, $N=7$) which does not have a spin-5/2 ground state in the cascade from spin-7/2 to spin-1/2.

(f) Ground states that are accidentally degenerate for all values of J always have the same total spin, but usually have space symmetries corresponding to different k-vectors. The *sc* lattice is the only cluster that has no "accidental" degeneracies in the ground state.

(g) At $J = 0$ there are some solutions with additional accidental degeneracies. The degenerate states contain mixtures of different total spin. These special solutions are summarized in Table IX.

There are many magnetic solutions to the t–t'–J model. Hund's empirical rules[47] may be employed to explain the occurence of ferrimagnetism for $N = 4$ and $N = 5$, but, as the filling increases, many-body effects overwhelm the system and the one-electron picture loses its predictive power. The $N = 7$ cases verify Nagaoka's theorem,[14] but the ferromagnetic state is quite unstable with respect to the interaction

parameter J, with a rapid level crossing to a lower spin state. Geometry also plays a role, as the *sc* and *fcc* lattices exhibit far stronger magnetic properties than the *bcc* or *sq* lattices.

The case with two holes ($N = 6$) has a spin-quenched ground state for all four different geometries. This fact has been observed for many geometries by previous investigators in small cluster calculations.[25–27,29–31,33] There are also variational and heuristic arguments why the two-hole state cannot be ferromagnetic.[17,51] Our solutions (Table VII) show one interesting additional feature: The ground-state manifold always contains a state with ${}^1\Gamma_1$ symmetry whenever the hypotheses of Nagaoka's theorem[14] are satisfied ($t' \leq 0$ for the *sc*, *bcc*, *fcc* ($t < 0$), and *sq* lattices). This result suggests that there is a two-hole extension to Nagaoka's theorem which yields a spin-singlet ground state. We leave this result as a conjecture, however, and do not offer any proof.

Up to this point we have kept the electron occupation number N fixed. It is important, however, to examine the stability of a fixed-N ground state with respect to discommensuration (a macroscopic rearrangement of the crystal into domains, with different electron number in each domain, but with an *average* filling N). The stability of a particular ground state (for fixed interaction J) is determined by forming the convex hull of the ground-state energy versus electron filling and comparing it to the calculated ground-state energy for N electrons. If the convex hull is lower in energy, then the ground state with N electrons is unstable against discommensuration. Previous work[33] on the phenomenon of discommensuration has concentrated exclusively on one and two holes in the half-filled band of a square lattice (determining the binding energy of hole pairs).

Our results are summarized in the form of phase diagrams (Figs. 5-9). The phase diagrams plot regions of parameter space that are stable against discommensuration as functions of the electron filling N (y-axis) and the Heisenberg interaction J (x-axis).

Horizontal solid lines denote stable ground-state solutions for fixed N. Dotted vertical lines separate regions where discommensuration occurs and also denote regions where the ground state for fixed N has a level crossing (see Tables V-VIII). The level crossings for fixed N are also marked by a solid dot in the phase diagrams.

In general, the tendency toward discommensuration increases as the interaction J increases; however, there are cases where islands of stable ground-state configurations form (these include $N = 4$ in the *bcc*, *fcc* ($t < 0$), and *sq* lattices, and $N = 7$ in the *fcc* ($t < 0$) lattice). The role of geometry on the structure of the phase diagrams can be explained by three empirical rules (listed in order of importance): (1) ground-state solutions with even numbers of electrons are more stable than solutions with odd numbers of electrons (in particular, $N = 0$, $N = 2$, and $N = 8$ are always stable); (2) filled or half-filled one-electron shells are stable in relation to other electron fillings; and (3) when the ground state for an odd number of electrons (N) is stable, the ground states for even numbers of electrons ($N \pm 1$) are also stable. In particular, the third rule implies that whenever an (N = odd) solution becomes unstable with respect to discommensuration, it always separates into even mixtures of solutions with ($N \pm 1$) electrons. However, when an (N = even) solution becomes unstable, it separates into many different kinds of mixtures ($N \pm 2$; $N+2, N-4$; $N+2, N-1$; $N+4, N-2$). These empirical rules explain the stability of $N = 0, 1, 2, 4, 5, 6, 8$ for the *sc* lattice; $N = 0, 1, 2, 8$ for the *bcc* and *sq* ($t' = 0$) lattices; $N = 0, 1, 2, 6, 8$ for the *fcc* ($t > 0$) and *sq* ($t' > 0$) lattices; $N = 0, 2, 3, 4, 6, 8$ for the *fcc* ($t < 0$) lattice; and $N = 0, 1, 2, 4, 8$ for the *sq* ($t' < 0$) lattice. The rules do not explain the stability of $N = 6, 7$ in the *bcc* lattice or $N = 7$ in the *fcc* ($t < 0$) lattice. We believe the last feature arises from many-body effects and a sensitivity of the solutions to the next-nearest-neighbor hopping t'. The *bcc* and *fcc* ($t < 0$) lattices are strongly sensitive to t', the *sq* lattice is moderately sensitive to t', and the *sc* and *fcc* ($t > 0$) lattices are insensitive to t'. Finally, we note that although the *sq* lattice does show regions of

parameter space which favor pair-formation of holes in the half-filled band, it is the *fcc* lattice with $t > 0$ ($t < 0$) that shows the strongest tendency toward hole (electron) pair-formation in the t–t'–J model. This result suggests that frustration is a key element for stable pair-formation in itinerant interacting electronic systems and that the *fcc* lattice is *more* likely to be superconducting than the *sq* lattice for a single-band model.

IV. Results: Heavy-Fermion Behavior

Two electrons which have strong correlation (*i.e.*, satisfy the "super" Pauli principle) must avoid each other when moving in a solid. This places an additional constraint on the electron dynamics which should, in turn, strongly affect the transport properties; *e.g.* reduce the specific heat, electron conductivity, etc. The constraint is felt in many-body solutions by a drastic reduction in the number of available states (reduced by one order of magnitude in eight-site clusters). Under certain circumstances, however, some transport properties are *enhanced* by orders of magnitude because of strong correlation (as evidenced in the HF materials[2,3]). We find analogous behavior in the many-body solutions to the t–t'–J model on small clusters.

The HF materials exhibit large coefficients of the term linear in the temperature in their specific heat, quasi-elastic magnetic excitations (large magnetic susceptibilities), and poor metallic conductivity. We test our solutions to the t–t'–J model to find candidate solutions that depict this HF behavior. Since electron correlation effects begin to be large at $N \simeq 4$, we expect solutions near half-filling to have the strongest HF character.

The large coefficient of the linear term in the specific heat arises from an abundance of low-lying excitations, *i.e.* many-body states in the ground-state manifold and energetically close to it. We calculated the maximum number of states (including all degeneracies) lying within an energy of $0.1\,|t|$ of the ground state for $0.0 \leq J < 1.0$

(see Table X). The maximum number of states appear for only a finite range of J, as illustrated for the three cases in Figs. 10-12. We search for enhancements[52] in the strong-correlation regime by comparing the maximum number of states in Table X with the total number of states in the ground-state manifold of the non-interacting regime (Table XI). The degeneracy of the non-interacting ground-state manifold is determined by a paramagnetic[53] filling of the one-electron levels of Table IV (all of the excited states in the non-interacting electron spectrum lie beyond $0.1|t|$ of the ground state). The possible HF lie predominantly near half-filling and are highlighted in boldface in Table X. Both the *bcc* and the *sq* ($t' = 0$) lattices show no tendency toward HF behavior due, in part, to the large density of states of the non-interacting electrons at half-filling.

Large magnetic susceptibilities and large magnetic fluctuations occur whenever two states with different total spin are nearly degenerate. These fluctuations increase when more than two different total-spin configurations are nearly degenerate (a feature that we call the spin-pileup effect). Many solutions exhibit this spin-pileup effect: the case of a half-filled band has, for all structures, five different total-spin configurations degenerate at $J = 0$; for $N = 7$, the spin-pileup effect is seen in the *sc* ($t' \leq 0$), *bcc* ($t' = 0$), *fcc* ($t > 0$), and *sq* lattices; for $N = 6$ and $N = 4$ it is observed in the *fcc* ($t > 0$) lattice and in the *sc* ($t' = 0$) lattice, respectively. A simple example of the spin-pileup effect is illustrated in Fig. 11. Cases when only two different total-spin states are nearly degenerate occur in the regions near isolated level crossings between the two states. These regions have been summarized in Tables V-VIII.

Finally, we require candidate HF solutions to exhibit weak metallic conductivity. Previous investigations[31] have shown that electrons in the strongly correlated regime are poor conductors (in particular, the half-filled band has electrons that are frozen in space, *i.e.* an insulator). We expect, however, an enhancement of the conductivity whenever a solution is close to a discommensuration instability, since the system has

states with two different charge distributions which are nearly degenerate.

Solutions to the t–t'–J model that satisfy all three criteria[54] are the best candidates for models of HF systems. These solutions are listed in Table XII. The solutions lie predominantly near half-filling, are quite sensitive to variations in J, are moderately sensitive to changes in t', and may be magnetic. In fact, the geometrical tendency toward HF appears to be closely linked to the geometrical tendency toward magnetism of the previous section, with the *sc* and *fcc* lattices having stronger HF character than the *bcc* and *sq* lattices.

Conclusions

We have studied the effect of geometry on the *exact* many-body solutions of the t–t'–J model in eight-site small clusters. We examined five particular cases: *sc*; *bcc*; *fcc* ($t > 0$); *fcc* ($t < 0$); and *sq* lattices. Spin and space-group symmetries were used to reduce the Hamiltonian to block-diagonal form, which decreased the diagonalization time by six orders of magnitude.

The spatial symmetry, k-vector, and total spin of the ground state were calculated for all electron fillings as a function of the interaction strength. We found that the ground state typically has minimal spin and there are many accidental degeneracies. Magnetic solutions (including ferromagnetism) occur in some cases when $J \ll t$. In particular, we verified Nagaoka's theorem,[14] found the ferromagnetic solutions to be quite unstable with respect to increasing J, and we proposed an extension of the theorem to the case of two holes: Whenever the hypotheses of Nagaoka's theorem[14] are satisfied and there are exactly two holes in the half-filled band, then the ground state is a spin-singlet with ${}^1\Gamma_1$ symmetry. This conjectured extension of Nagaoka's theorem indicates that the ferromagnetic solution is quite unstable to both interaction strength J and electron filling N.

We studied the stability of the many-body solutions with respect to discommensuration. Amazingly enough, we found that the phase diagrams can be almost entirely described by a one-electron picture: The stability of solutions tends to decrease as the interaction J is increased; the one-eighth ($N=2$) and one-half ($N=8$) filled bands are always stable; an even number of electrons tends to be more stable than an odd number; and an odd number of electrons that forms a half-filled one-electron shell tends to be stable. Frustration was a key element to the binding of two holes or two electrons, as shown in the *fcc* lattice. In particular, we found no evidence for enhanced superconductivity (via the binding of holes) in the two-dimensional *sq* lattice versus the three-dimensional lattices.

Heavy-fermion behavior was studied by examining the character of the ground-state manifold and its low-lying excitations. We found many-body solutions that have a large density of many-body states near the ground state, have large spin fluctuations, and are poor metallic conductors. These solutions exhibit HF character for only a small range of the interaction and are sometimes magnetic.

Geometry plays a similar role in both magnetism and HF behavior. The *sc* and *fcc* lattices have a stronger tendency toward magnetism and HF behavior than the *bcc* and *sq* lattices.

In conclusion, the small-cluster technique is an alternate approach to the many-body problem that treats electron correlation effects exactly, but has uncontrolled finite-size effects. Group theory is used to simplify the problem, so that many different cases can be studied. We find a richness to the structure of the ground-state solutions as functions of the interaction strength, electron filling, and geometry, that includes magnetism and HF behavior.

Acknowledgments

We acknowledge helpful discussions with T. Barbee, C. Chen, D. Chrzan, A. Garcia, and A. Maiti. We thank A. Reich for providing us with his computer codes which were used in the early stages of this project. One of the authors (J.K.F.) also acknowledges the support of the Department of Education. This research was supported, at the Lawrence Berkeley Laboratory, by the Director, Office of Energy Research, Office of Basic Energy Sciences, Materials Science Division, U.S. Department of Energy, under contract No. DE-AC03-76SF00098.

Appendix

The cubic point group O_h has 48 operations, however, the improper rotations and inversion yield no additional information when spherically symmetric orbitals are placed at each lattice site. Therefore, the relevant cubic point group for the small clusters that we study is the orthogonal group O which has 24 operations. Similarly, the relevant point group for the square lattice is C_{4v} which has 8 operations. The eight-site cluster has eight translations which yield space groups of order 192 (64) for the cubic (square) lattices. However, it turns out that there is a fourfold redundancy of group operations in the *sc* lattice when spherically symmetric orbitals are placed at the lattice sites (a similar phenomenon occurs in the four-site tetrahedral cluster[28]). This reduces the order of the space group for the *sc* cluster to 48 and this reduced group is isomorphic to the point group O_h with an origin at the center of the cube.

The *sc* Brillouin zone[43] is sampled at four symmetry stars: Γ (d=1); R (d=1); M (d=3); and X (d=3). The character table[43] is reproduced in Table A1 with the conventional and the space group notations for the 10 irreducible representations.

The *bcc* and *fcc* lattices display the full symmetry of the proper space group. Their Brillouin zones[43] are sampled at three symmetry stars: Γ (d=1); H (d=1); and N (d=6) for the *bcc* lattice and Γ (d=1); X (d=3); and L (d=4) for the *fcc* lattice. The

character tables[43] are reproduced in Tables A2 and A3. The space group operations are denoted by a point group operation with origin at site 1 and a translation vector. Nearest-neighbor translations are denoted by τ and next-nearest neighbor translations by θ. The subscripts $\|$, $\perp$, and $\angle$ refer to translations that are parallel to, perpendicular to, or at an angle to the rotation axis of the point group operation.

The *sq* lattice also displays the full symmetry of the proper space group. The Brillouin zone[43] is sampled at four symmetry stars: Γ (d=1); M (d=1); X (d=2); and Σ (d=4). The character table[43] is reproduced in Table A4. The symbol σ denotes reflections in the planes perpendicular to the x- and y-axes, σ' denotes reflections in planes perpendicular to the diagonals $x \pm y$, Ω denotes the third-nearest-neighbor translations, and the subscripts $\|$ ($\perp$) refer to translations that are parallel (perpendicular) to the normal of the mirror plane.

Finally, we elaborate upon the algebraic identification of the lattice points in an infinite lattice with those of an eight-site cluster with PBC. A *sc* lattice is described by triples of integers (i,j,k). The eight-site *sc* cluster with PBC describes the same set of points, but each point on the infinite lattice is identified with one of eight equivalence classes, determined by the site in the small cluster with which it is equivalent. These equivalence classes are given in Table A.5 for the *sc*, *bcc*, *fcc*, and *sq* lattices.

References

1 R. M. White, *Quantum Theory of Magnetism,* (McGraw-Hill, New York, 1970).

2 G.R. Stewart, Rev. Mod. Phys. **56,** 755 (1984).

3 P. Fulde, J. Keller, and G. Zwicknagl, Solid State Phys. **41,** 1 (1988).

4 J.G. Bednorz and K.A. Müller, Z. Phys. B **64,** 189 (1986); M.K. Wu, J.R. Ashburn, C.J. Torng, P.H. Hor, R.L. Meng, L. Gao, Z.J. Huang, Y.Q Wang, and C.W. Chu, Phys. Rev. Lett. **58,** 908 (1987).

[5] P.W. Anderson, Science **235,** 1196 (1987); C.M. Varma, S. Schmitt-Rink, and E. Abrahams, Solid State Com. **62,** 681 (1987); V.J. Emery, Phys. Rev. Lett. **58,** 2794 (1987); F.C. Zhang and T.M. Rice, Phys. Rev. B **37,** 3759 (1988).

[6] The summations in Eq. (2) run over all nearest-neighbor i,j (*i.e.*, each pair is counted twice) to guarantee hermiticity of the Hamiltonian.

[7] J. Hubbard, Proc. R. Soc. London, Ser. A **276,** 238 (1963); *ibid.*, **277,** 237 (1964); *ibid.*, **281,** 401 (1964); *ibid.*, **285,** 542 (1965); *ibid.*, **296,** 82 (1967); *ibid.*, **296,** 100 (1967).

[8] P.W. Anderson, Solid State Phys. **14,** 99 (1963).

[9] J.R. Schrieffer and P.A. Wolff, Phys. Rev. **149,** 491 (1966).

[10] A.B. Harris and R.V. Lange, Phys. Rev. **157,** 295 (1967).

[11] A.H. MacDonald, S.M. Girvin, and D. Yoshioka, Phys. Rev. B **37,** 9753 (1988); A.M. Oleś, *ibid.*, **41,** 2562 (1990); A.H. MacDonald, S.M. Girvin, and D. Yoshioka, *ibid.*, **41,** 2565 (1990).

[12] W. Marshall, Proc. R. Soc. London, Ser. A **232,** 48 (1955); E.H. Lieb and D.C. Mattis, J. Math. Phys. **3,** 749 (1962).

[13] E.H. Lieb, Phys. Rev. Lett. **62,** 1201 (1989).

[14] Y. Nagaoka, Solid State Com. **3,** 409 (1965); D.J. Thouless, Proc. Phys. Soc. London **86,** 893 (1965); Y. Nagaoka, Phys. Rev. **147,** 392 (1966); H. Tasaki, Phys. Rev. B **40,** 9192 (1989).

[15] E.H. Lieb and D.C. Mattis, Phys. Rev. **125,** 164 (1962).

[16] E.H. Lieb and F.Y. Wu, Phys. Rev. Lett. **20,** 1445 (1968).

[17] B. Doucot and X.G. Wen, Phys. Rev. B **40,** 2719 (1989).

[18] M. Ogata and H. Shiba, Phys. Rev. B **41,** 2326 (1990).

[19] B. Sutherland, Phys. Rev. B **12,** 3795 (1975); P. Schlottman, *ibid.,* **36,** 5177 (1987); *ibid.,* **41,** 4164 (1990); M. Kotrla, Phys. Lett. A **145,** 33 (1990); P.A. Bares and G. Blatter, ETH-TH/89-54, *preprint,* (1990).

[20] For a review see L.M. Falicov in *Recent Progress in Many-Body Theories* Vol. 1, A.J. Kallio, E. Pajanne, and R.F. Bishop, eds. (Plenum Publishing Corp., New York, 1988) p. 275; J. Callaway, Physica B **149,** 17 (1988).

[21] L.M. Falicov, *Group theory and Its Physical Applications,* (University of Chicago Press, Chicago, 1966) p. 144ff.

[22] L.M. Falicov and R.A. Harris, J. Chem. Phys. **51,** 3153 (1969).

[23] O.J. Heilmann and E.H. Lieb, Trans. NY Acad. Sci. **33,** 116 (1971).

[24] H. Shiba and P.A. Pincus, Phys. Rev. B **5,** 1966 (1972); K.-H. Heinig and J. Monecke, Phys. Stat. Sol. B **49,** K139 (1972); *ibid.* **49,** K141 (1972); *ibid.* **50,** K117 (1972); H. Shiba, Prog. Theor. Phys. **48,** 2171 (1972); D. Cabib and T.A. Kaplan, Phys. Rev. B **7,** 2199 (1973).

[25] M. Takahashi, Phys. Soc. Japan **47,** 47 (1979).

[26] A. Kawabata, Solid State Com. **32,** 893 (1979); A. Kawabata in *Electron Correlation and Magnetism in Narrow Band Systems,* T. Moriya, ed. (Springer, New York, 1981) p. 172.

[27] J. Callaway, D.P. Chen, and Y. Zhang, Phys. Rev. B **36,** 2084 (1987).

[28] A.M. Oleś, B. Oleś, and K.A. Chao, J. Phys. C **13,** L979 (1980); J. Rössler, B. Fernandez, and M. Kiwi, Phys. Rev. B **24,** 5299 (1981); D.J. Newman, K.S. Chan, and B. Ng, J. Phys. Chem. Solids **45,** 643 (1984); L.M. Falicov and R.H. Victora, Phys. Rev. B **30,** 1695 (1984); C.M. Willet and W.-H. Steeb, J. Phys. Soc. Japan **59,** 393 (1990).

[29] M. Takahashi, J. Phys. Soc. Japan **51,** 3475 (1982).

[30] Y. Ishii and S. Sugano, J. Phys. Soc. Japan **53,** 3895 (1984); J. Callaway, D.P. Chen, and R. Tang, J. Phys. D **3,** 91 (1986); Phys. Rev. B **35,** 3705 (1987); J. Callaway, *ibid.,* **35,** 8723 (1987); W. Pesch, H. Büttner, and J. Reichl, *ibid.,* **37,** 5887 (1988); J. Callaway, D.P. Chen, Q. Li, D.G. Kanhere, and P. Misra, *preprint;* J. Callaway, D.P. Chen, D.G. Kanhere, and Q.Li, *preprint.*

[31] A. Reich and L.M. Falicov, Phys. Rev. B **37,** 5560 (1988); *ibid.,* **38,** 11199 (1988).

[32] C. Chen, A. Reich, and L.M. Falicov, Phys. Rev. B **38,** 12823 (1988); C. Chen, Phys. Lett. A **142,** 271 (1989).

[33] E. Kaxiras and E. Manousakis, Phys. Rev. B **37,** 656 (1988); X. Zotos, *ibid.,* **37,** 5594 (1988); E. Kaxiras and E. Manousakis, *ibid.,* **38,** 866 (1988); J. Bonca, P. Prelovsek, and I. Sega, *ibid.,* **39,** 7074 (1989); J.A. Riera and A.P. Young, *ibid.,* **39,** 9697 (1989); *ibid.,* **40,** 5285 (1989); E. Dagotto, A. Moreo, and T. Barnes, *ibid.,* **40,** 6721 (1989); Y. Fang, A.E. Ruckenstein, E. Dagotto, and S. Schmitt-Rink, *ibid.* **40,** 7406 (1989); Y. Hasegawa and D. Poilblanc, *ibid.,* **40,** 9035 (1989); Int. J. Mod. Phys. B **3,** 1853 (1989); A. Parola, S. Sorella, S. Baroni, M. Parrinello, and E. Tosatti, *ibid.,* **3,** 139 (1989); M. Imada and Y. Hatsugai, J. Phys. Soc. Japan **58,** 3752, (1989); E. Dagotto, A. Moreo, R.L. Sugar, and D. Toussaint, Phys. Rev. B **41,** 811 (1990); D. Poilblanc, Y. Hasegawa, and T.M. Rice, *ibid.,* **41,** 1949 (1990); K.-H. Luk and D.L. Cox, *ibid.,* **41,** 4456 (1990); V. Elser, D.A. Huse, B.I. Schraiman, and E.D. Siggia, *ibid.,* **41,** 6715 (1990); D. Poilblanc and Y. Hasegawa, *ibid.,* **41,** 6989 (1990).

[34] R. H. Victora and L.M. Falicov, Phys. Rev. Lett. **55,** 1140 (1985); E.C. Sowa and L.M. Falicov, Phys. Rev. B **35,** 3765 (1987).

[35] A. Reich and L.M. Falicov, Phys. Rev. B **37,** 5560 (1988); E.C. Sowa and L.M. Falicov, *ibid.,* **37,** 8707 (1988).

[36] C. Chen and L.M. Falicov, Phys. Rev. B **40,** 3560 (1989); C. Chen, Phys. Rev. Lett. **64,** 2176 (1990).

[37] C. Chen, Phys. Rev. B **41,** 1320 (1990).

[38] M. Ogata and H. Shiba, J. Phys. Soc. Japan, **57,** 3074 (1988); H. Shiba and M. Ogata, J. Magn. and Magn. Mat. **76 & 77,** 59 (1988); W.H. Stephan, W. v.d. Linden and P. Horsch, Phys. Rev. B **39,** 2924 (1989); M. Ogata and H. Shiba J. Phys. Soc. Japan **58,** 2836 (1989); Physica C **158,** 355 (1989); D.M. Frenkel, R.J. Gooding, B.I. Shraiman, E.D. Siggia, Phys. Rev. B **41,** 350 (1990); M.S. Hybertsen, *private communication.*

[39] M. Tinkham, *Group Theory and Quantum Mechanics,* (McGraw-Hill Book Company, New York, 1964) p. 20ff.; p. 80ff.

[40] L.M. Falicov, *Group Theory and Its Physical Applications,* (The University of Chicago Press, Chicago, 1966) p. 20ff.; p. 46ff.

[41] A.W. Luehrmann, Adv. in Phys. **17,** 1 (1968).

[42] G. Burns and A.M. Glazer, *Space Groups for Solid State Scientists,* (Academic Press, New York, 1978) p. 213ff.

[43] L.P. Bouckaert, R. Smoluchowski, and E. Wigner, Phys. Rev. **50,** 58 (1936).

[44] J.H. Wilkinson and C. Reinsch, *Handbook for Automatic Computation, Vol. II: Linear Algebra,* ed. F.L. Bauer, (Springer-Verlag, New York, 1971) p. 227.

[45] Although the eigenvalue spectra is symmetric with respect to the sign of t, the symmetry label for many-body states with odd numbers of electrons may depend on the sign of t.

[46] T. Oguchi and H. Kitatani, J. Phys. Soc. Japan **58,** 1403 (1989); R. Saito, Sol. St. Commun. **72,** 517 (1989).

[47] F. Hund, *Linienspektren und Periodisches System der Elemente,* (Springer, Berlin, 1927), p. 124; E.U. Condon and G.H. Shortley, *The Theory of Atomic Spectra,*

(Cambridge University Press, Cambridge, 1957), p. 209.

[48] Our results agree with the work of Riera and Young in Ref. 32 except in the $N = 6$ case we find the spin-2 state lower in energy than the spin-1 state (rather than degenerate in energy) when $J = 0$.

[49] We denote solutions with maximum spin as ferromagnetic.

[50] We denote solutions with neither maximal nor minimal spin as ferrimagnetic, regardless of the spin-spin correlation functions (which we have not computed).

[51] P.W. Anderson, B.S. Shastry, and D. Hristopulos, Phys. Rev. B **40,** 8939 (1989); B. Doucot and R. Rammal, Int. J. Mod. Phys. B **3,** 1755 (1989); B.S. Shastry, H.R. Krishnamurthy, and P.W. Anderson, Phys. Rev. B **41,** 2375 (1990); A. Basile and V. Elser, Phys. Rev. B **41,** 4842 (1990).

[52] There is a finite-size effect that can be very strong in the non-interacting case — it occurs whenever a one-electron shell is filled. The non-interacting solution is then an insulator with only one state in the ground-state manifold. In this case (and in the fillings near the closed shell) the strongly correlated solutions will undoubtedly be HF. We do not exclude these potential HF unless they fail to satisfy the additional criteria.

[53] Comparisons can be made with respect to ferromagnetic filling of the one-electron levels (which spans a Hilbert space with the same dimension as the strongly correlated Hilbert space) but none of the HF are eliminated from such a comparison (the finite-size effect is much stronger in this case).

[54] The HF with $N = 3$ is near a discommensuration instability and may be too good a conductor. The HF with $N = 4$ is stable against discommensuration but is probably metallic since strong-correlation effects are not expected to reduce drastically the electronic conductivity in a quarter-filled band. We do not discard either solution.

Table I. Hamiltonian block sizes for N electrons in an eight-site cluster in the strongly interacting limit (no double-occupation of a lattice site).

N	Dimension of Hilbert Space
0	1
1	16
2	112
3	448
4	1120
5	1792
6	1792
7	1024
8	256

Table II. Largest Hamiltonian block sizes for N electrons in the four different eight-site clusters when expanded in a symmetrized basis of definite spin and spatial symmetry.

N	*sc*	*bcc*	*fcc*	*sq*
0	1	1	1	1
1	1	1	1	1
2	3	2	2	3
3	8	5	5	8
4	16	8	9	14
5	18	9	12	18
6	18	9	11	18
7	8	5	5	8
8	3	2	2	3

Table III. Renormalized parameters for the t–t'–J Hamiltonian when restricted to isolated eight-site lattices.

	sc	*bcc*	*fcc*	*sq*
1NN	$2t$	$2t$	$2t$	t
2NN	$4t'$	$2t'$	$6t'$	$2t'$
int	$2J$	$2J$	$2J$	J

Table IV. One-electron energy levels for the four different eight-site clusters.

sc	*bcc*	*fcc*	*sq*
$E_\Gamma = -6t-12t'$	$E_\Gamma = -8t-6t'$	$E_\Gamma = -12t-6t'$	$E_\Gamma = -4t-4t'$
$E_X = -2t+4t'$	$E_N = 2t'$	$E_L = 6t'$	$E_\Sigma = 0$
$E_M = 2t+4t'$	$E_H = 8t-6t'$	$E_X = 4t-6t'$	$E_X = 4t'$
$E_R = 6t-12t'$			$E_M = 4t-4t'$

Table V. Ground-state symmetry for the $N = 4$ case. The symmetry labels refer to the irreducible representations of the space group (see the appendix) with the superscript corresponding to the spin-degeneracy $(2S+1)$. The critical values of J/t record the parameter values where a level crossing occurs within the interval $0.0 \leq J/t < 1.0$.

	$t' > 0$			$t' = 0$			$t' < 0$		
	sym.	deg.	$[J/t]_{crit.}$	sym.	deg.	$[J/t]_{crit.}$	sym.	deg.	$[J/t]_{crit.}$
sc	$^1\Gamma_{12}$	2		$^5R_2$	5	0.13715	$^5R_2$	5	0.21162
				$^1\Gamma_{12}$	2		$^1\Gamma_{12}$	2	
	$^1\Gamma_{12}\oplus{}^1H_{12}$	4	0.07807	$^1\Gamma_{12}\oplus{}^1H_{12}$	4	0.11379	$^3H'_{25}\oplus{}^3N_3$	27	0.03743
bcc	$^1\Gamma'_{25}\oplus{}^1N_2$	9		$^1\Gamma'_{25}\oplus{}^1N_2$	9		$^1\Gamma_{12}\oplus{}^1H_{12}$	4	0.09289
							$^1\Gamma'_{25}\oplus{}^1N_2$	9	
fcc	$^3X_5$	18	0.00273	$^3X_5$	18	0.00521	$^3X_5$	18	0.00788
$(t>0)$	$^1\Gamma'_{25}\oplus{}^1X_3$	6		$^1\Gamma'_{25}\oplus{}^1X_3$	6		$^1\Gamma'_{25}\oplus{}^1X_3$	6	
fcc	$^3X_2$	9	0.06404	$^3X_2$	9	0.08559	$^3X_2$	9	0.07870
$(t>0)$	$^1\Gamma_{12}$	2		$^1\Gamma_{12}$	2	0.69025	$^1\Gamma_{12}$	2	0.33435
				$^1L_2$	4		$^1L_2$	4	
	$^3\Gamma_5\oplus{}^3X_3$	12	0.00274	$^1\Gamma_1\oplus{}^1\Gamma_4\oplus{}^1M_1\oplus{}^1M_4$	4	0.11379	$^3M_3$	3	0.08520
sq	$^1\Gamma_4\oplus{}^1M_4$	2	0.08861	$^1\Gamma_3\oplus{}^1M_5\oplus{}^1X_4\oplus{}^1\Sigma_2$	9		$^1\Gamma_3$	1	
	$^1M_5\oplus{}^1X_4$	4							

Table VI. Ground-state symmetry for the $N = 5$ case.

	$t' > 0$			$t' = 0$			$t' < 0$		
	sym.	deg.	$[J/t]_{crit.}$	sym.	deg.	$[J/t]_{crit.}$	sym.	deg.	$[J/t]_{crit.}$
sc	$^4R_2$	4	0.22719	$^4R_2$	4	0.28014	$^4R_2$	4	0.30507
	$^2X_2$	6		$^2X_2$	6		$^2X_2$	6	
bcc	$^2N_1 \oplus {}^2N_4$	24	0.13027	$^2N_1 \oplus {}^2N_4$	24	0.21214	$^2N_1 \oplus {}^2N_4$	24	0.20073
	$^2\Gamma'_{15} \oplus {}^2H'_{15}$			$^2\Gamma'_{15} \oplus {}^2H'_{15} \oplus {}^2N_2 \oplus {}^2N_3$	36		$^2\Gamma'_{15} \oplus {}^2H'_{15} \oplus {}^2N_2 \oplus {}^2N_3$	36	0.82705
	$\oplus {}^2N_2 \oplus {}^2N_3$	36					$^2\Gamma'_{25} \oplus {}^2N_2$	18	
fcc	$^4L_2$	16	0.00216	$^4L_2$	16	0.00432	$^4L_2$	16	0.00690
($t > 0$)	$^2L_3$	16		$^2L_3$	16		$^2L_3$	16	
fcc	$^2X_1$	6	0.65744	$^2X_1$	6	0.52150	$^2X_1$	6	0.30260
($t < 0$)	$^2L_3$	16	0.85651	$^2X_5$	12		$^2X_5$	12	
	$^2X_5$	12							
	$^2\Sigma_1$	8	0.16958	$^2X_1 \oplus {}^2X_2 \oplus {}^2\Sigma_1 \oplus {}^2\Sigma_2$	24	0.21214	$^2X_1$	4	0.27940
sq	$^2\Sigma_2$	8		$^2\Gamma_2 \oplus {}^2\Gamma_5 \oplus {}^2M_2 \oplus {}^2M_5$			$^2\Sigma_2$	8	
				$\oplus {}^2X_3 \oplus {}^2X_4 \oplus 2{}^2\Sigma_2$	36				

Table VII. Ground-state symmetry for the $N = 6$ case.

	$t' > 0$			$t' = 0$			$t' < 0$		
	sym.	deg.	$[J/t]_{crit.}$	sym.	deg.	$[J/t]_{crit.}$	sym.	deg.	$[J/t]_{crit.}$
sc	$^1\Gamma_{12}$	2		$^1\Gamma_1$	1	0.04489	$^1\Gamma_1$	1	0.21765
				$^1\Gamma_{12}$	2		$^1\Gamma_{12}$	2	
	$^1\Gamma_1 \oplus {}^1\Gamma_{12} \oplus {}^1H_2$	4	0.13007	$^1\Gamma_1 \oplus {}^1\Gamma_{12} \oplus {}^1H_2$	4	0.21355	$^1\Gamma_1 \oplus {}^1\Gamma_{12} \oplus {}^1H_2$	4	0.20287
bcc	$^1\Gamma'_{25} \oplus {}^1N_2$	9		$^1\Gamma'_{25} \oplus {}^1N_2$	9		$^1\Gamma'_{25} \oplus {}^1N_2$	9	0.54656
							$^1\Gamma_1$	1	
fcc ($t > 0$)	$^1\Gamma_{12}$	2		$^1\Gamma_{12}$	2		$^1\Gamma_{12}$	2	
	$^1\Gamma_1$	1	0.63022	$^1\Gamma_1$	1	0.49013	$^1\Gamma_1$	1	0.30941
fcc	$^1\Gamma'_{25} \oplus {}^1X_3$	6		$^1\Gamma'_{25} \oplus {}^1X_3$	6	0.80484	$^1\Gamma'_{25} \oplus {}^1X_3$	6	0.42641
($t < 0$)				$^1L_2$	4		$^1L_2$	4	0.78826
							$^1\Gamma_1 \oplus {}^1\Gamma_{12}$	3	
sq	$^1\Gamma_1$	1	0.17094	$2{}^1\Gamma_1 \oplus {}^1\Gamma_4 \oplus {}^1M_4$	4	0.21355	$^1\Gamma_1$	1	0.28349
	$^1\Gamma_3$	1		$^1\Gamma_3 \oplus {}^1M_5 \oplus {}^1X_4 \oplus {}^1\Sigma_2$	9		$^1M_5 \oplus {}^1X_4$	4	

Table VIII. Ground-state symmetry for the $N = 7$ case.

	$t' > 0$			$t' = 0$			$t' < 0$		
	sym.	deg.	$[J/t]_{crit.}$	sym.	deg.	$[J/t]_{crit.}$	sym.	deg.	$[J/t]_{crit.}$
sc	$^2X_1$	6		$^8R_1$	8	0.05878	$^8R_1$	8	0.11763
				$^2X_1$	6		$^6\Gamma_1$	6	0.14158
							$^4R_1$	4	0.27134
							$^2X_1$	6	0.34310
							$^2\Gamma_1$	2	
bcc	$^6N_1$	36	0.02488	$^8H_1$	8	0.10383	$^8H_1$	8	0.14286
	$^4\Gamma_{12}\oplus{}^4H_{12}$	16	0.09174	$^6N_1$	36	0.11856	$^6\Gamma_1$	6	0.20000
	$^2N_1$	12		$^4\Gamma_{12}\oplus{}^4H_{12}$	16	0.16573	$^4H_1$	4	0.33333
				$^2N_1$	12		$^2\Gamma_1$	2	
fcc ($t > 0$)	$^2\Gamma_2\oplus{}^2X_1\oplus{}^2X_2$	14		$^2\Gamma_2\oplus{}^2X_1\oplus{}^2X_2$	14		$^2\Gamma_2\oplus{}^2X_1\oplus{}^2X_2$	14	
fcc ($t < 0$)	$^8\Gamma_1$	8	0.08785	$^8\Gamma_1$	8	0.12633	$^8\Gamma_1$	8	0.14286
	$^6L_1$	24	0.11555	$^6L_1$	24	0.17794	$^6X_1$	18	0.20000
	$^4\Gamma'_{25}\oplus{}^4X_3$	24	0.22932	$^4\Gamma'_{25}\oplus{}^4X_3$	24	0.20209	$^4\Gamma_1\oplus{}^4\Gamma_{12}\oplus{}^4X_1$	24	0.33333
	$^2L_1$	8	0.26969	$^4L_3$	32	0.25000	$^2X_1\oplus{}^2X_2$	12	
	$^2X_5$	12	0.34658	$^4\Gamma_1\oplus{}^4\Gamma_{12}\oplus{}^4X_1$	24	0.33333			
	$^2L_2\oplus{}^2L_3$	24	0.69048	$^2X_1\oplus{}^2X_2$	12				
	$^2X_1\oplus{}^2X_2$	12							
sq	$^8M_1$	8	0.03336	$^8M_1$	8	0.10383	$^8M_1$	8	0.13165
	$^6X_1$	12	0.05991	$^6X_1\oplus{}^6\Sigma_1$	36	0.11856	$^4\Gamma_4\oplus{}^4M_4$	8	0.19593
	$^4\Gamma_1\oplus{}^4M_1$	8	0.12436	$^4\Gamma_1\oplus{}^4\Gamma_4\oplus{}^4M_1\oplus{}^4M_4$	16	0.16573	$^2\Sigma_1$	8	0.53125
	$^2X_1$	4		$^2X_1\oplus{}^2\Sigma_1$	12		$^2\Gamma_1$	2	

Table IX. Accidental degeneracies in the t–t'–J model at $J = 0$.

lattice	N	ground state	deg.
fcc ($t < 0$)	2	${}^3X_2 \oplus {}^1\Gamma_{12}$	11
bcc $t' = 0$	4	${}^3H'_{25} \oplus {}^3N_3 \oplus {}^1\Gamma_{12} \oplus {}^1H_{12}$	31
sq $t' = 0$	4	${}^3\Gamma_5 \oplus {}^3M_3 \oplus {}^3X_3 \oplus {}^3\Sigma_2$ $\oplus {}^1\Gamma_1 \oplus {}^1\Gamma_4 \oplus {}^1M_1 \oplus {}^1M_4$	31
fcc ($t > 0$)	6	${}^5\Gamma_2 \oplus {}^3X_2 \oplus {}^1\Gamma_{12}$	16
fcc ($t > 0$)	7	${}^6X_2 \oplus {}^4L_2 \oplus {}^4\Gamma_{12} \oplus {}^4X_1 \oplus {}^4X_2$ $\oplus {}^2L_3 \oplus {}^2\Gamma_2 \oplus {}^2X_1 \oplus {}^2X_2$	96
all	8	*all*	256

Table X. Maximum number of many-body states lying within $0.1|t|$ of the ground-state energy (including the degeneracy of the ground-state manifold). Potential HF are highlighted in bold.

N	*sc*			*bcc*			*fcc* ($t > 0$)			*fcc* ($t < 0$)			*sq*		
t'	+	0	-	+	0	-	+	0	-	+	0	-	+	0	-
1		2			2			2			6			2	
2		1			1			1			11			1	
3	4	4	**18**		12			8			10		8	12	4
4	11	**16**	7		40			24			11		18	40	4
5		10			60			32		**28**	**34**	**34**	16	60	**12**
6	2	3	3		13			16		**7**	**10**	**10**	2	13	**5**
7	6	**38**	**18**	52	60	14		**96**		**48**	**98**	**42**	28	76	**54**
8		**256**			256			**256**			**256**		**256**	256	**256**

Table XI. Maximum number of non-interacting-electron states lying within $0.1|t|$ of the ground-state energy (including the degeneracy of the ground-state manifold).

N	*sc*			*bcc*			*fcc* ($t > 0$)			*fcc* ($t < 0$)			*sq*		
t'	+	0	-	+	0	-	+	0	-	+	0	-	+	0	-
1		2			2			2			6			2	
2		1			1			1			15			1	
3		6			12			8			20		8	12	4
4		15			66			28			15		28	66	6
5		20			220			56			6		56	220	4
6		15			495			70			1		70	495	1
7		6			792			56			8		56	792	8
8		1			924			28			28		28	924	28

Table XII. Many-body solutions to the t–t'–J model that exhibit strong HF character. The range of interaction strength J/t where the solutions are HF and the total spin of the ground state S_{GS} are included.

N	lattice	t'	J/t	S_{GS}
3	*sc*	$t' < 0$	$0.0 < J/t < 0.05$	1/2
4	*sc*	$t' = 0$	$0.0 < J/t < 0.04$	2 or 0
7	*sc*	$t' = 0$	$0.05 < J/t < 0.065$	7/2 or 1/2
7	*sc*	$t' < 0$	$0.12 < J/t < 0.13$	7/2 or 5/2
7	*fcc* ($t > 0$)	*all* t'	$0.0 < J/t < 0.01$	1/2
7	*fcc* ($t < 0$)	$t' > 0$	$0.1 < J/t < 0.12$	5/2 or 3/2
7	*fcc* ($t < 0$)	$t' = 0$	$0.17 < J/t < 0.19$	5/2 or 3/2
7	*sq*	$t' < 0$	$0.15 < J/t < 0.16$	3/2

Table A1. Character table for the space group of the eight-site *sc* cluster. The space group is isomorphic to the cubic point group O_h, with an origin at the center of the small cluster, when spherically symmetric orbitals are placed at the lattice sites. E is the identity, C_n^m is the rotation of $2\pi m/n$ about an n-fold axis, and J is the inversion. Both the space group and the point group notations for the irreducible representations are included.

		1	3	6	6	8	1	3	6	6	8
		E	C_4^2	C_4	C_2	C_3	J	JC_4^2	JC_4	JC_2	JC_3
Γ_1	A_{1g}	1	1	1	1	1	1	1	1	1	1
Γ_2	A_{2g}	1	1	-1	-1	1	1	1	-1	-1	1
Γ_{12}	E_g	2	2	0	0	-1	2	2	0	0	-1
M_2	T_{1g}	3	-1	1	-1	0	3	-1	1	-1	0
M_1	T_{2g}	3	-1	-1	1	0	3	-1	-1	1	0
R_2	A_{1u}	1	1	1	1	1	-1	-1	-1	-1	-1
R_1	A_{2u}	1	1	-1	-1	1	-1	-1	1	1	-1
R_{12}	E_u	2	2	0	0	-1	-2	-2	0	0	1
X_1	T_{1u}	3	-1	1	-1	0	-3	1	-1	1	0
X_2	T_{2u}	3	-1	-1	1	0	-3	1	1	-1	0

Table A2. Character table for the space group of the eight-site *bcc* cluster. The space group operations are constructed by a point group operation with origin at site 1 followed by a translation. The symbol 0 denotes no translation, τ denotes a nearest-neighbor translation, and θ is a next-nearest-neighbor translation. The subscripts $\parallel$, $\perp$, and $\angle$ refer to translations that are parallel to, perpendicular to, and at an angle to the rotation axis of the point group operation.

	1	6	24	12	32	4	12	24	12	12	32	3	6	12
	E	C_4^2	C_4	C_2	C_3	E	C_4^2	C_4	C_2	C_2	C_3	E	C_4^2	C_2
	0	$0\theta_{\parallel}$	0θ	$0\theta_{\perp}$	0θ	τ	τ	τ	$\tau_{\angle}$	$\tau_{\perp}$	τ	θ	$\theta_{\perp}$	$\theta_{\angle}$
Γ_1	1	1	1	1	1	1	1	1	1	1	1	1	1	1
Γ_2	1	1	-1	-1	1	1	1	-1	-1	-1	1	1	1	-1
Γ_{12}	2	2	0	0	-1	2	2	0	0	0	-1	2	2	0
Γ_{15}'	3	-1	1	-1	0	3	-1	1	-1	-1	0	3	-1	-1
Γ_{25}'	3	-1	-1	1	0	3	-1	-1	1	1	0	3	-1	1
H_1	1	1	1	1	1	-1	-1	-1	-1	-1	-1	1	1	1
H_2	1	1	-1	-1	1	-1	-1	1	1	1	-1	1	1	-1
H_{12}	2	2	0	0	-1	-2	-2	0	0	0	1	2	2	0
H_{15}'	3	-1	1	-1	0	-3	1	-1	1	1	0	3	-1	-1
H_{25}'	3	-1	-1	1	0	-3	1	1	-1	-1	0	3	-1	1
N_1	6	2	0	2	0	0	0	0	0	0	0	-2	-2	-2
N_2	6	-2	0	0	0	0	0	0	-2	2	0	-2	2	0
N_3	6	-2	0	0	0	0	0	0	2	-2	0	-2	2	0
N_4	6	2	0	-2	0	0	0	0	0	0	0	-2	-2	2

Table A3. Character table for the space group of the eight-site *fcc* cluster. The notation is identical to that of Table A.2.

	1	6	24	12	32	6	6	12	24	24	1	12	32
	E	C_4^2	C_4	C_2	C_3	E	C_4^2	C_4^2	C_4	C_2	E	C_2	C_3
	0	0θ	$0\theta\tau_\perp$	$0\tau_\parallel$	$0\tau_\perp$	τ	$\tau_\perp$	τ_L	τ_L	τ_L	θ	$\theta\tau_\perp$	$\theta\tau_L$
Γ_1	1	1	1	1	1	1	1	1	1	1	1	1	1
Γ_2	1	1	-1	-1	1	1	1	1	-1	-1	1	-1	1
Γ_{12}	2	2	0	0	-1	2	2	2	0	0	2	0	-1
Γ_{15}'	3	-1	1	-1	0	3	-1	-1	1	-1	3	-1	0
Γ_{25}'	3	-1	-1	1	0	3	-1	-1	-1	1	3	1	0
X_1	3	3	1	1	0	-1	-1	-1	-1	-1	3	1	0
X_2	3	3	-1	-1	0	-1	-1	-1	1	1	3	-1	0
X_3	3	-1	-1	1	0	-1	3	-1	1	-1	3	1	0
X_4	3	-1	1	-1	0	-1	3	-1	-1	1	3	-1	0
X_5	6	-2	0	0	0	-2	-2	2	0	0	6	0	0
L_1	4	0	0	2	1	0	0	0	0	0	-4	-2	-1
L_2	4	0	0	-2	1	0	0	0	0	0	-4	2	-1
L_3	8	0	0	0	-1	0	0	0	0	0	-8	0	1

Table A4. Character table for the space group of the eight-site *sq* cluster. The symbol σ denotes the mirror planes perpendicular to the $x-$ and $y-$axes and σ' denotes the mirror planes perpendicular to the diagonals $x \pm y$. The translations are denoted by 0 (no translation), τ (nearest-neighbor translation), θ (next-nearest-neighbor), and Ω (third-nearest-neighbor). The subscripts $\parallel$ and $\perp$ refer to translations parallel to or perpendicular to the normals of the mirror planes.

Table A4

	1	8	2	4	4	4	8	4	4	4	8	2	2	4	4	1
	E	C_4	C_4^2	σ	σ'	E	C_4	C_4^2	σ	σ	σ'	E	C_4^2	σ	σ'	E
	0	$0\theta\Omega$	0Ω	0Ω	$0\theta_\perp$	τ	τ	τ	$\tau_\parallel$	$\tau_\perp$	τ	θ	θ	θ	$\theta_\parallel\Omega$	Ω
Γ_1	1	1	1	1	1	1	1	1	1	1	1	1	1	1	1	1
Γ_2	1	1	1	-1	-1	1	1	1	-1	-1	-1	1	1	-1	-1	1
Γ_3	1	-1	1	1	-1	1	-1	1	1	1	-1	1	1	1	-1	1
Γ_4	1	-1	1	-1	1	1	-1	1	-1	-1	1	1	1	-1	1	1
Γ_5	2	0	-2	0	0	2	0	-2	0	0	0	2	-2	0	0	2
M_1	1	1	1	1	1	-1	-1	-1	-1	-1	-1	1	1	1	1	1
M_2	1	1	1	-1	-1	-1	-1	-1	1	1	1	1	1	-1	-1	1
M_3	1	-1	1	1	-1	-1	1	-1	-1	-1	1	1	1	1	-1	1
M_4	1	-1	1	-1	1	-1	1	-1	1	1	-1	1	1	-1	1	1
M_5	2	0	-2	0	0	-2	0	2	0	0	0	2	-2	0	0	2
X_1	2	0	2	2	0	0	0	0	0	0	0	-2	-2	-2	0	2
X_2	2	0	2	-2	0	0	0	0	0	0	0	-2	-2	2	0	2
X_3	2	0	-2	0	0	0	0	0	-2	2	0	-2	2	0	0	2
X_4	2	0	-2	0	0	0	0	0	2	-2	0	-2	2	0	0	2
Σ_1	4	0	0	0	2	0	0	0	0	0	0	0	0	0	-2	-4
Σ_2	4	0	0	0	-2	0	0	0	0	0	0	0	0	0	2	-4

Table A5. Equivalence classes of the eight small-cluster sites in the *sc*, *bcc*, *fcc*, and *sq* infinite lattices.

Class	*sc*	*bcc*	*fcc*	*sq*
1	$(2i,2j,2k)$	$(4i,4j,4k)$	$(2i,2j,2k)$	$(2i,2j)$
		$(4i+2,4j+2,4k+2)$	$i+j+k$ = even	$i+j$ = even
2	$(2i+1,2j,2k)$	$(4i+2,4j,4k)$	$(2i,2j+1,2k+1)$	$(2i+1,2j)$
		$(4i,4j+2,4k+2)$	$i+j+k$ = even	$i+j$ = even
3	$(2i+1,2j+1,2k)$	$(4i,4j,4k+2)$	$(2i+1,2j,2k+1)$	$(2i+1,2j+1)$
		$(4i+2,4j+2,4k)$	$i+j+k$ = odd	$i+j$ = odd
4	$(2i,2j+1,2k)$	$(4i,4j+2,4k)$	$(2i+1,2j+1,2k)$	$(2i,2j+1)$
		$(4i+2,4j,4k+2)$	$i+j+k$ = odd	$i+j$ = even
5	$(2i+1,2j,2k+1)$	$(4i+1,4j+1,4k+1)$	$(2i,2j,2k)$	$(2i,2j)$
		$(4i+3,4j+3,4k+3)$	$i+j+k$ = odd	$i+j$ = odd
6	$(2i,2j,2k+1)$	$(4i+3,4j+1,4k+1)$	$(2i,2j+1,2k+1)$	$(2i+1,2j)$
		$(4i+1,4j+3,4k+3)$	$i+j+k$ = odd	$i+j$ = odd
7	$(2i,2j+1,2k+1)$	$(4i+1,4j+1,4k+3)$	$(2i+1,2j,2k+1)$	$(2i+1,2j+1)$
		$(4i+3,4j+3,4k+1)$	$i+j+k$ = even	$i+j$ = even
8	$(2i+1,2j+1,2k+1)$	$(4i+1,4j+3,4k+1)$	$(2i+1,2j+1,2k)$	$(2i,2j+1)$
		$(4i+3,4j+1,4k+3)$	$i+j+k$ = even	$i+j$ = odd

Figure Captions

Figure 1. Eight-site cluster with PBC for the *sc* lattice in a) real and b) reciprocal space. The nearest neighbors of the site 1 are *two* each of the sites 2, 4, and 6 as indicated in a). The four symmetry stars in b) are $\Gamma = (0,0,0)$; $R = (1,1,1)\,\pi/a$; $M = (1,1,0)\,\pi/a$; and $X = (1,0,0)\,\pi/a$.

Figure 2. Eight-site cluster with PBC for the *bcc* lattice in a) real and b) reciprocal space. The dotted line in a) is the body diagonal. The nearest neighbors of site 5 are *two* each of the sites 1, 2, 3, and 4. The three symmetry stars in b) are $\Gamma = (0,0,0)$; $H = (2,0,0)\,\pi/a$; and $N = (1,1,0)\,\pi/a$.

Figure 3. Eight-site cluster with PBC for the *fcc* lattice in a) real and b) reciprocal space. The double-tetrahedral structure is highlighted with dotted lines in a). The three symmetry stars in b) are $\Gamma = (0,0,0)$; $X = (0,0,2)\,\pi/a$; and $L = (1,1,1)\,\pi/a$.

Figure 4. Eight-site cluster with PBC for the *sq* lattice in a) real and b) reciprocal space. The $2\sqrt{2}a \times 2\sqrt{2}a$ "primitive" cell is highlighted with dotted lines in a). The four symmetry stars are $\Gamma = (0,0)$; $M = (1,1)\,\pi/a$; $X = (1,0)\,\pi/a$; and $\Sigma = (1,1)\,\pi/2a$.

Figure 5. Stability phase diagram for the *sc* lattice. The x-axis is the interaction strength J/t and the y-axis is the electron filling N. Solid horizontal lines correspond to stable single-phases. Dotted vertical lines denote discommensuration instabilities or level crossings in the fixed-N solutions. Level crossings are also marked by a black dot. Three cases have been calculated: a) $t' = 0.15\,|t|$; b) $t' = 0.0$; and c) $t' = -0.15\,|t|$.

Figure 6. Stability phase diagram for the *bcc* lattice. Three cases have been calculated: a) $t' = 0.5\,|t|$; b) $t' = 0.0$; and c) $t' = -0.5\,|t|$. Note the phase islands for $N = 4$.

Figure 7. Stability phase diagram for the *fcc* ($t > 0$) lattice. Three cases have been calculated: a) $t' = 0.15\,|t|$; b) $t' = 0.0$; and c) $t' = -0.15\,|t|$.

Figure 8. Stability phase diagram for the *fcc* ($t < 0$) lattice. Three cases have been calculated: a) $t' = 0.15|t|$; b) $t' = 0.0$; and c) $t' = -0.15|t|$. Note the phase islands for $N = 4$ and $N = 7$ and that $N = 1$ is unstable.

Figure 9. Stability phase diagram for the *sq* lattice. Three cases have been calculated: a) $t' = 0.15|t|$; b) $t' = 0.0$; and c) $t' = -0.15|t|$. Note the phase islands for $N = 4$.

Figure 10. Total number of states in the ground-state manifold and in the low-lying excitations within $0.1|t|$ of it for the *sc* ($t' < 0$) lattice and $N = 3$.

Figure 11. Total number of states in the ground-state manifold and in the low-lying excitations within $0.1|t|$ of it for the *fcc* ($t > 0$) lattice and $N = 7$. There are no low-lying excitations in the range $0.1 < J/t < 1.0$. The spin-pileup effect can be seen at $J = 0$.

Figure 12. Total number of states in the ground-state manifold and in the low-lying excitations within $0.1|t|$ of it for the *fcc* ($t < 0$) lattice with $t' = 0$ and $N = 7$. There are no low-lying excitations in the range $0.5 < J/|t| < 1.0$.

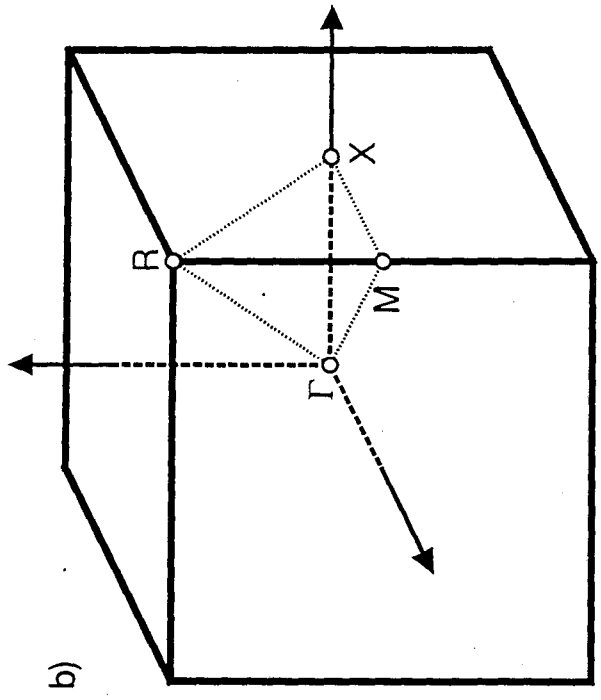

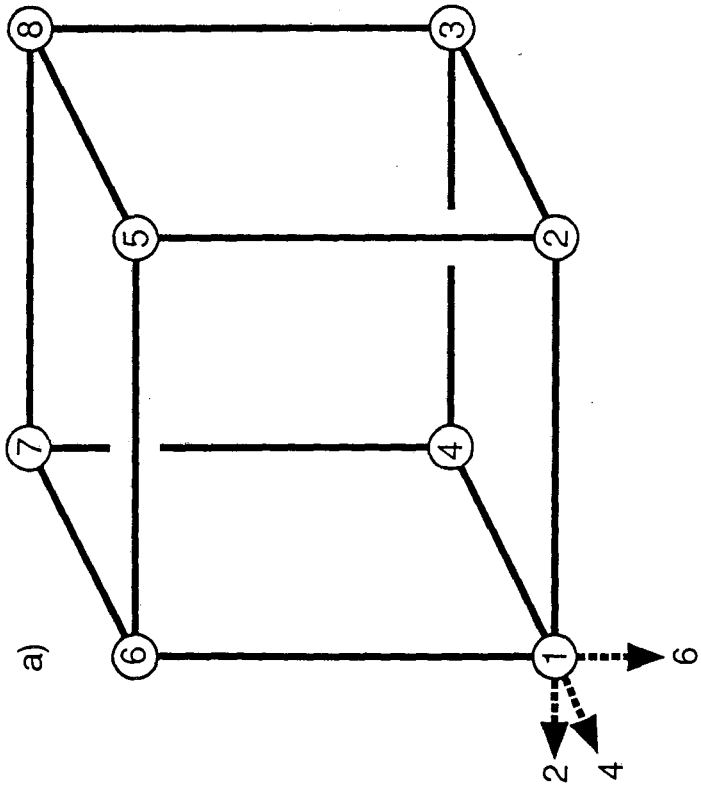

FIGURE 1

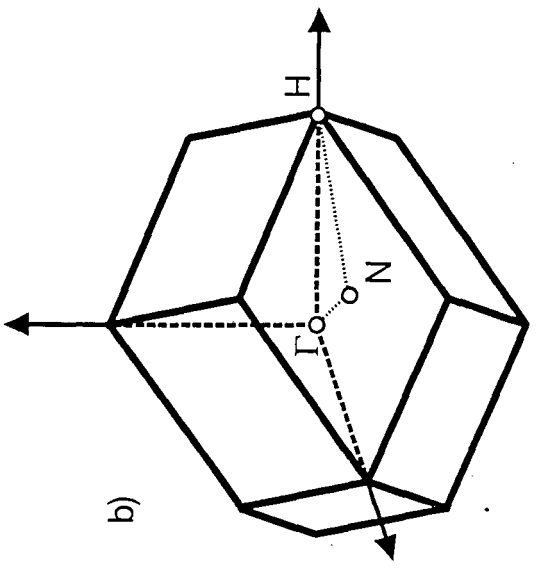

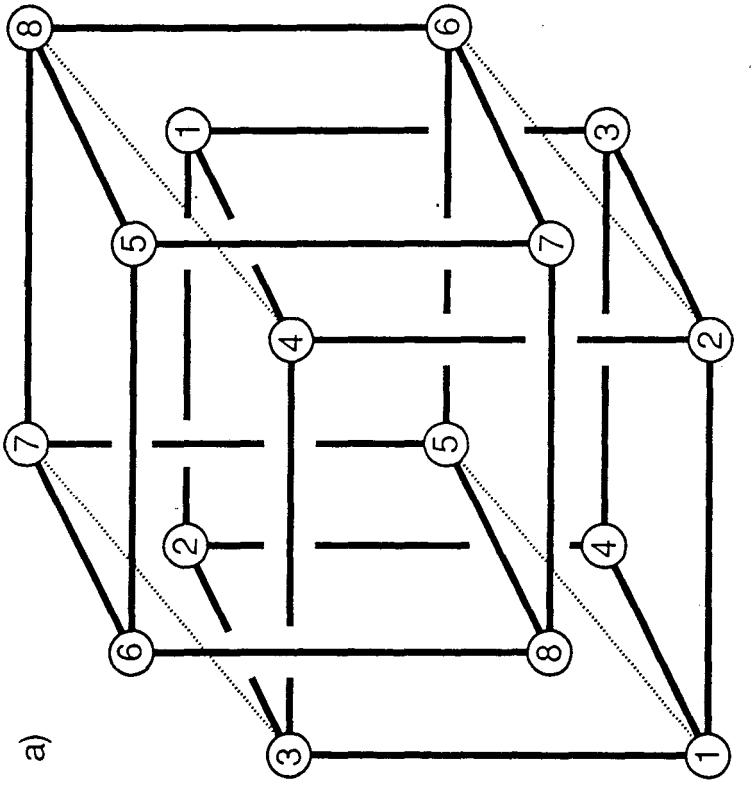

FIGURE 2

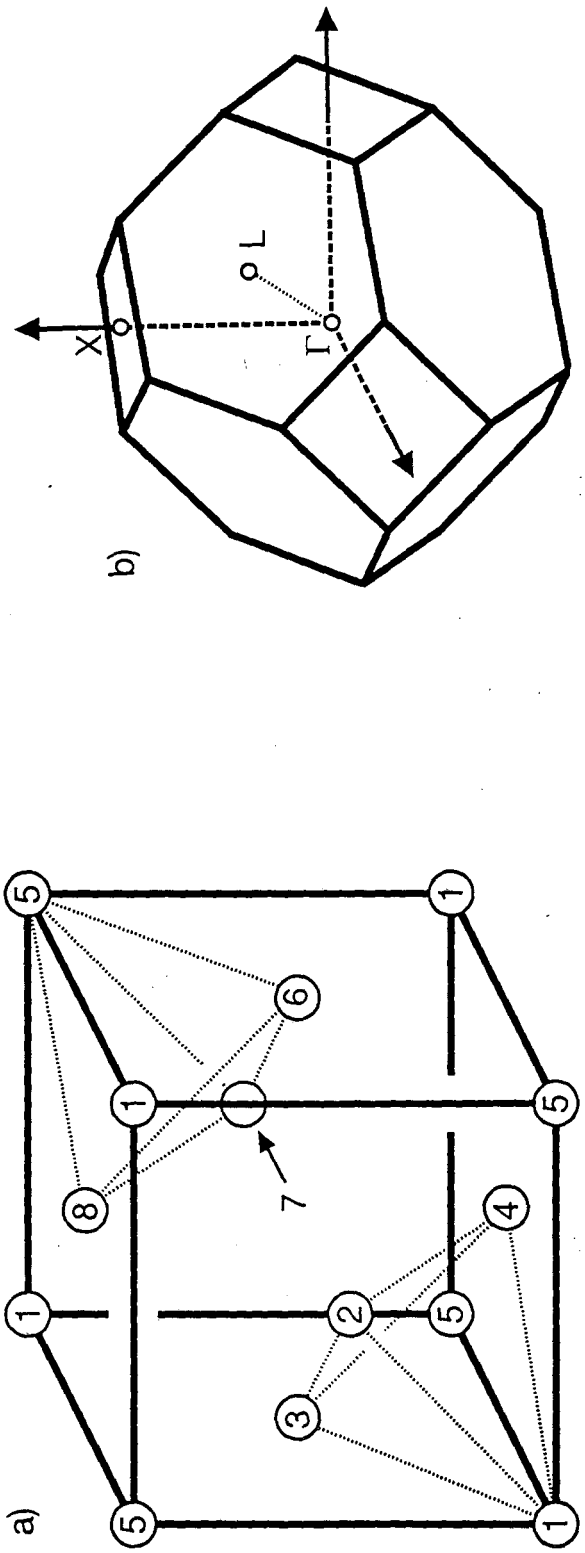

FIGURE 3

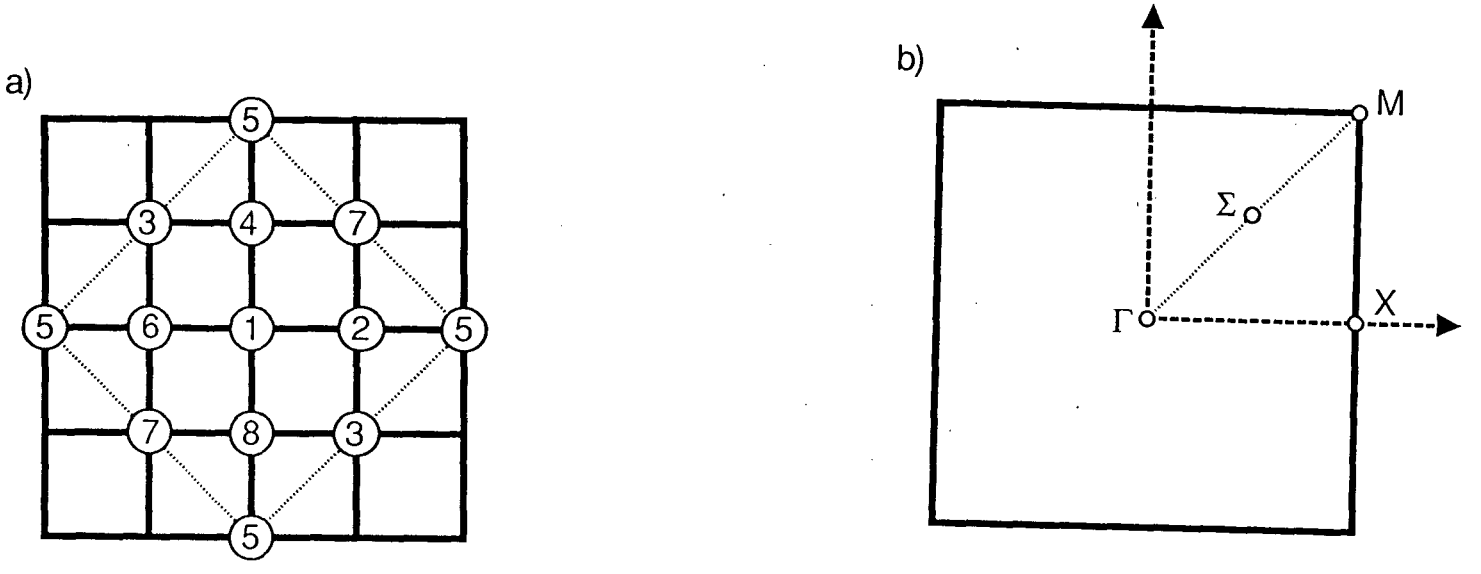

FIGURE 4

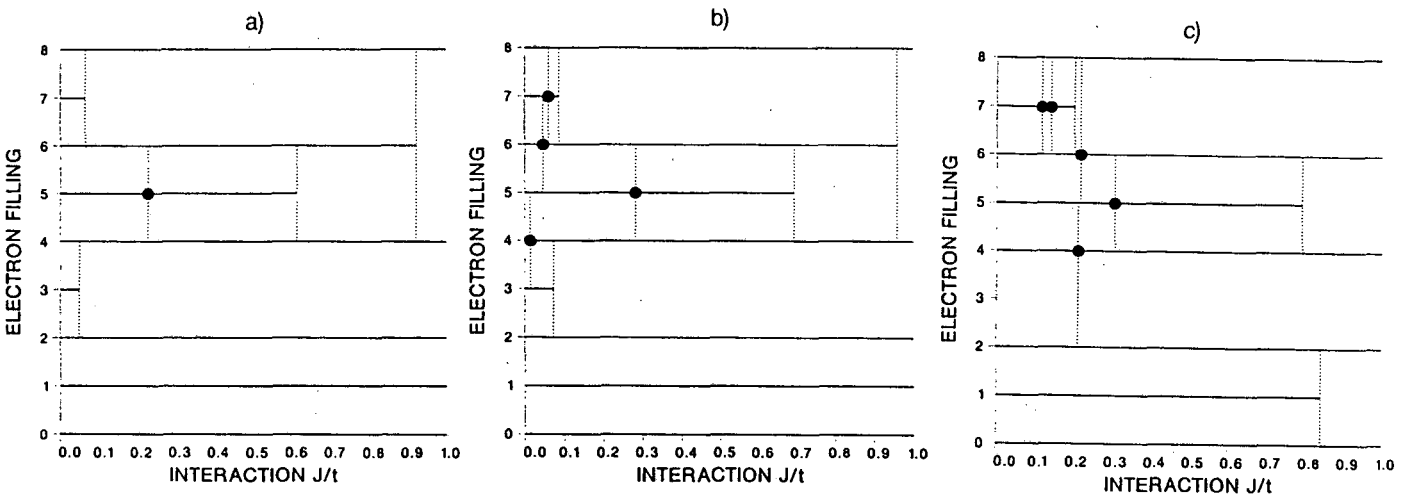
a)
b)
c)
ELECTRON FILLING
INTERACTION J/t
0 1 2 3 4 5 6 7 8
0.0 0.1 0.2 0.3 0.4 0.5 0.6 0.7 0.8 0.9 1.0

FIGURE 5

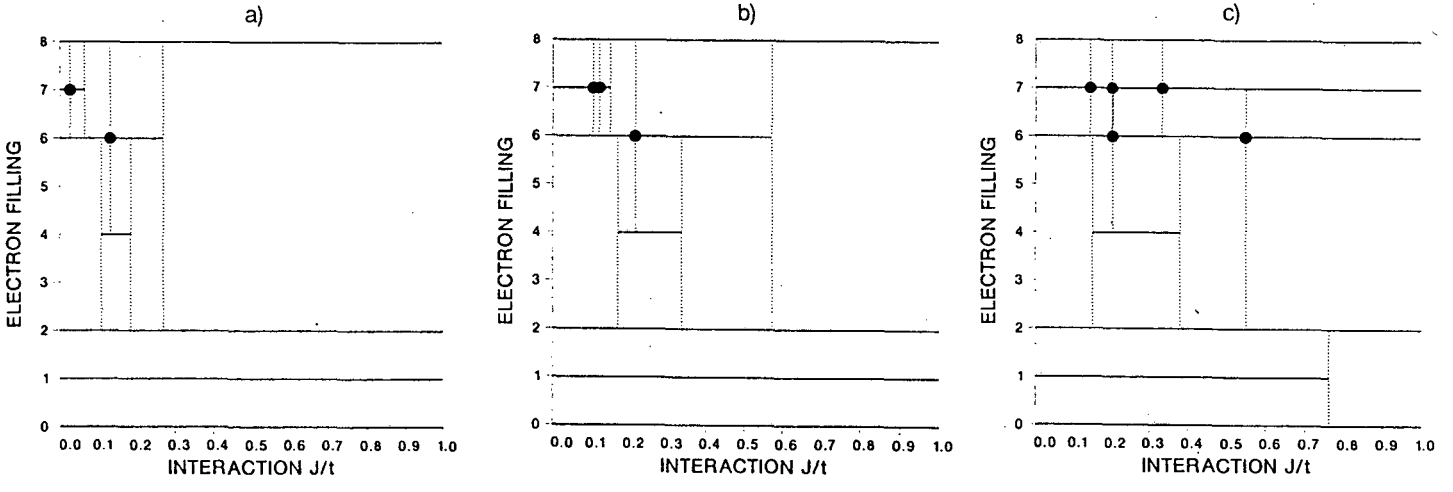
a)
b)
c)
ELECTRON FILLING
INTERACTION J/t
0 1 2 3 4 5 6 7 8
0.0 0.1 0.2 0.3 0.4 0.5 0.6 0.7 0.8 0.9 1.0

FIGURE 6

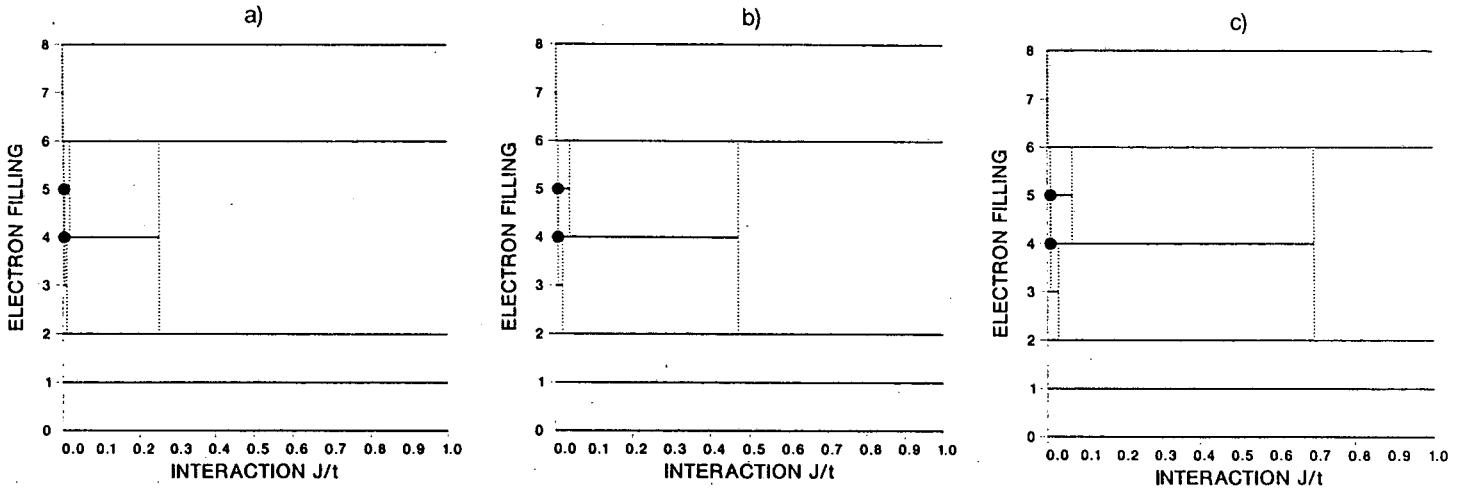
a)
b)
c)
ELECTRON FILLING
INTERACTION J/t
0 1 2 3 4 5 6 7 8
0.0 0.1 0.2 0.3 0.4 0.5 0.6 0.7 0.8 0.9 1.0

FIGURE 7

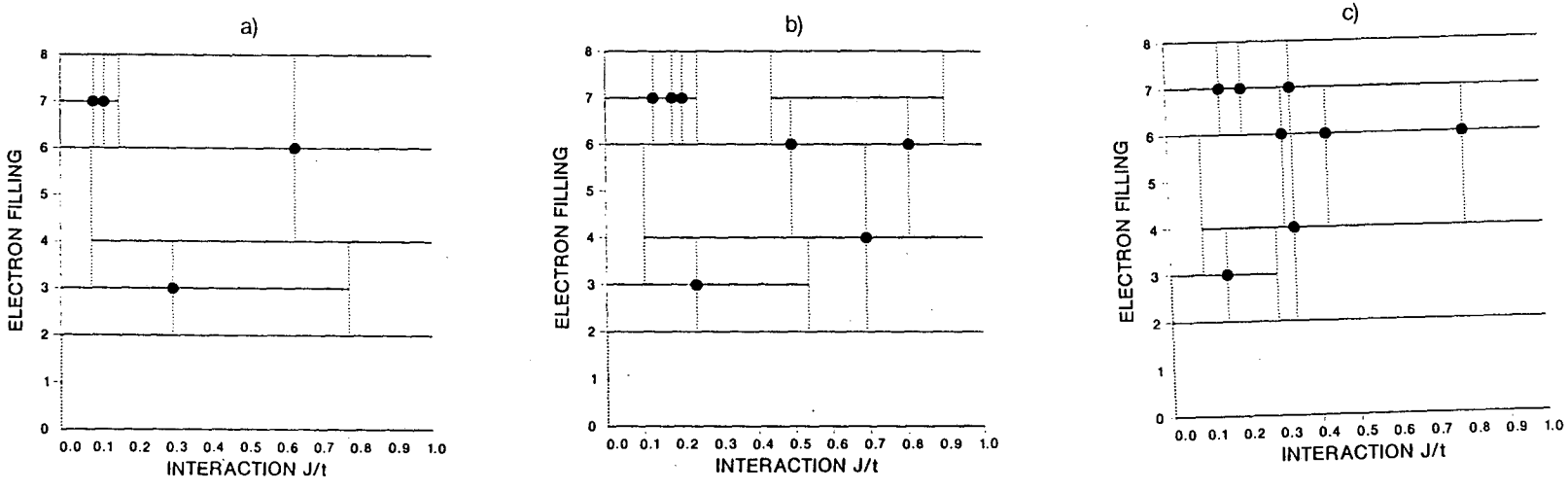
a)
b)
c)
ELECTRON FILLING
INTERACTION J/t
0 1 2 3 4 5 6 7 8
0.0 0.1 0.2 0.3 0.4 0.5 0.6 0.7 0.8 0.9 1.0

FIGURE 8

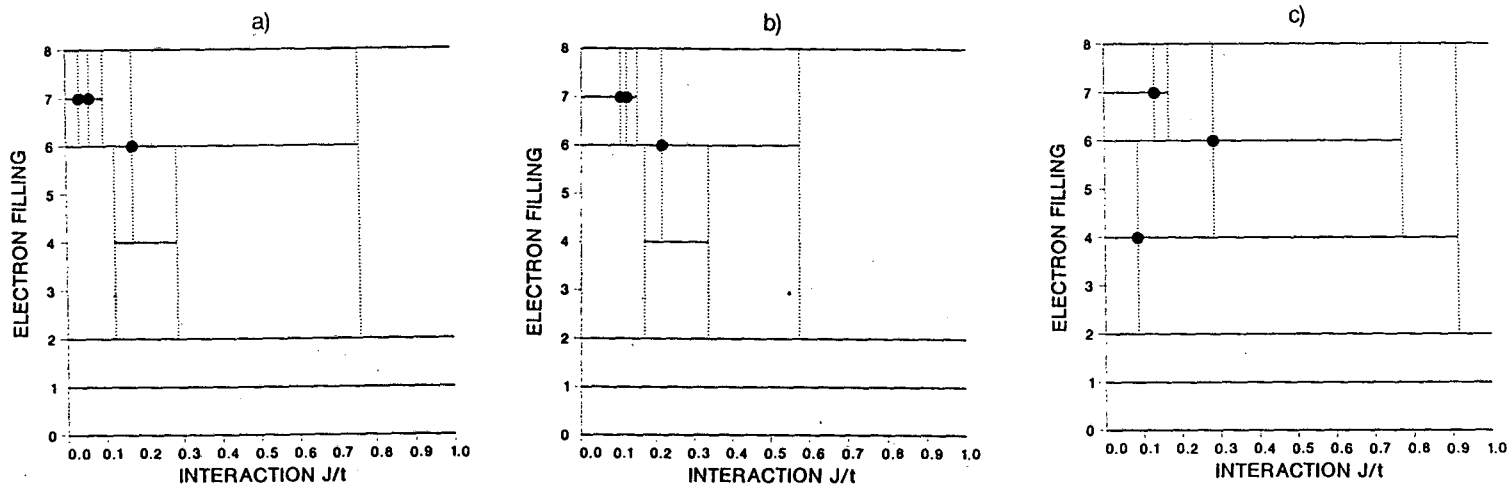
a)
b)
c)
ELECTRON FILLING
INTERACTION J/t
0 1 2 3 4 5 6 7 8
0.0 0.1 0.2 0.3 0.4 0.5 0.6 0.7 0.8 0.9 1.0

FIGURE 9

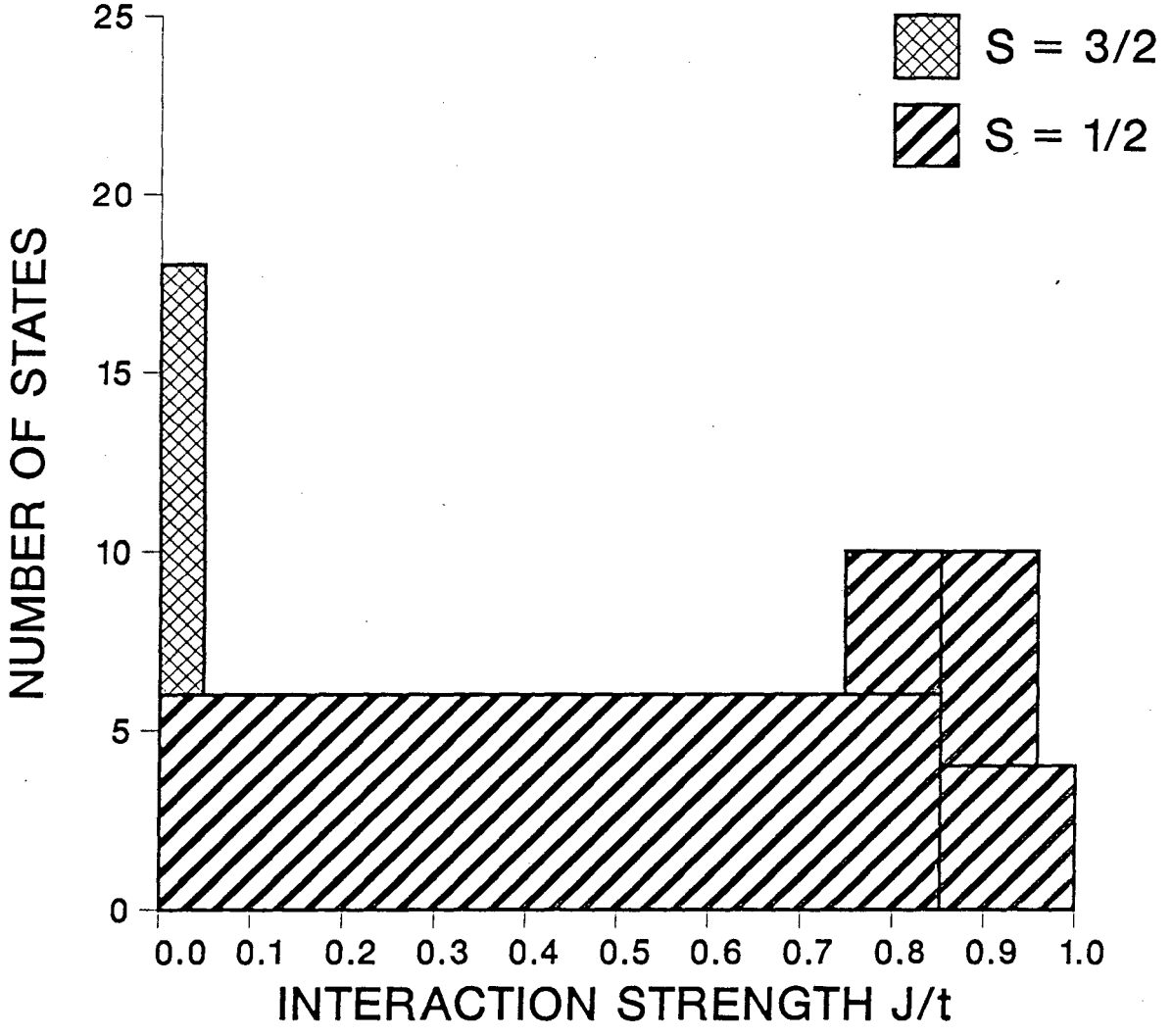
S = 3/2
S = 1/2
NUMBER OF STATES
25
20
15
10
5
0
0.0
0.1
0.2
0.3
0.4
0.5
0.6
0.7
0.8
0.9
1.0
INTERACTION STRENGTH J/t

FIGURE 10

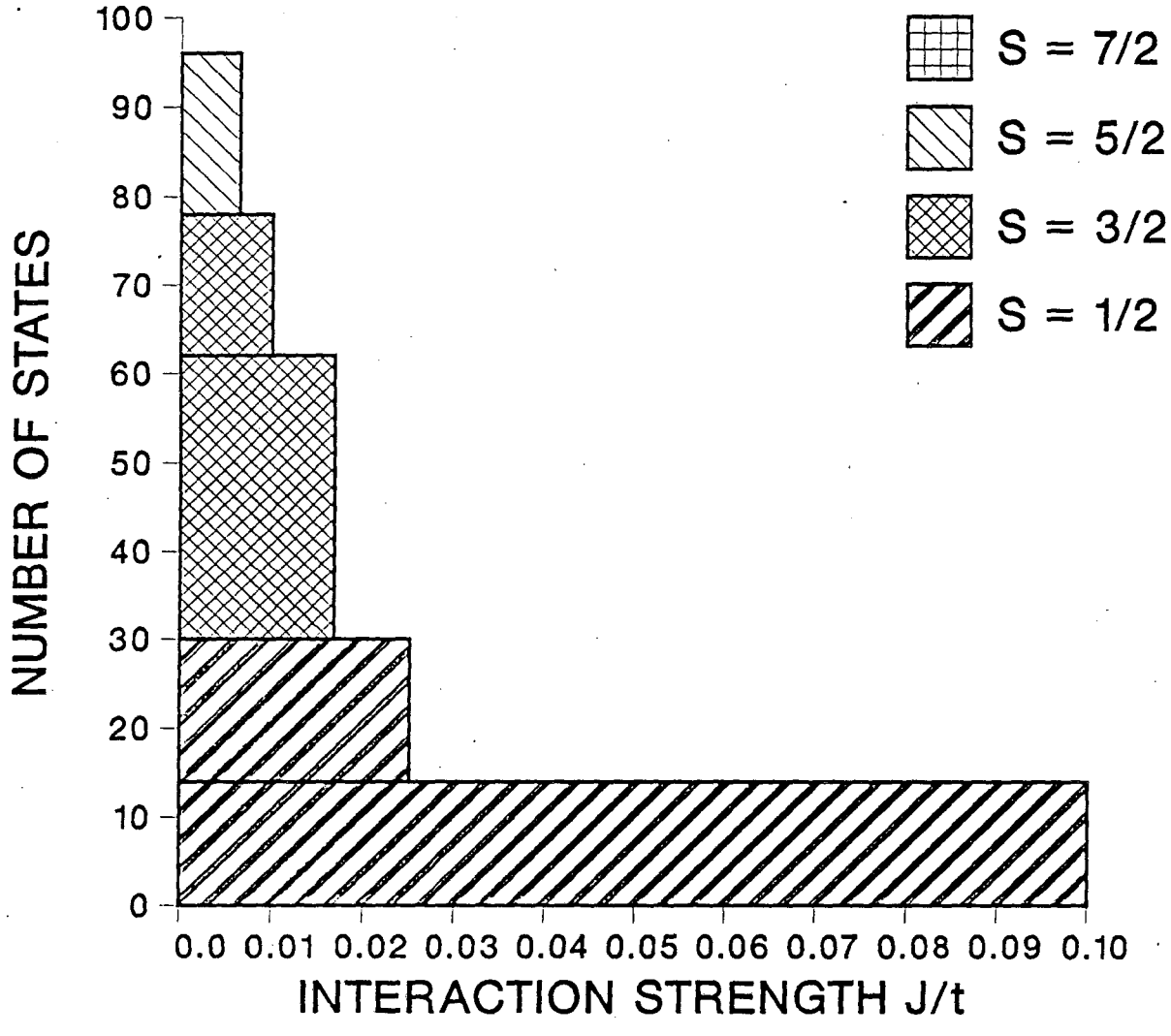
NUMBER OF STATES
100
90
80
70
60
50
40
30
20
10
0
0.0 0.01 0.02 0.03 0.04 0.05 0.06 0.07 0.08 0.09 0.10
INTERACTION STRENGTH J/t
S = 7/2
S = 5/2
S = 3/2
S = 1/2

FIGURE 11

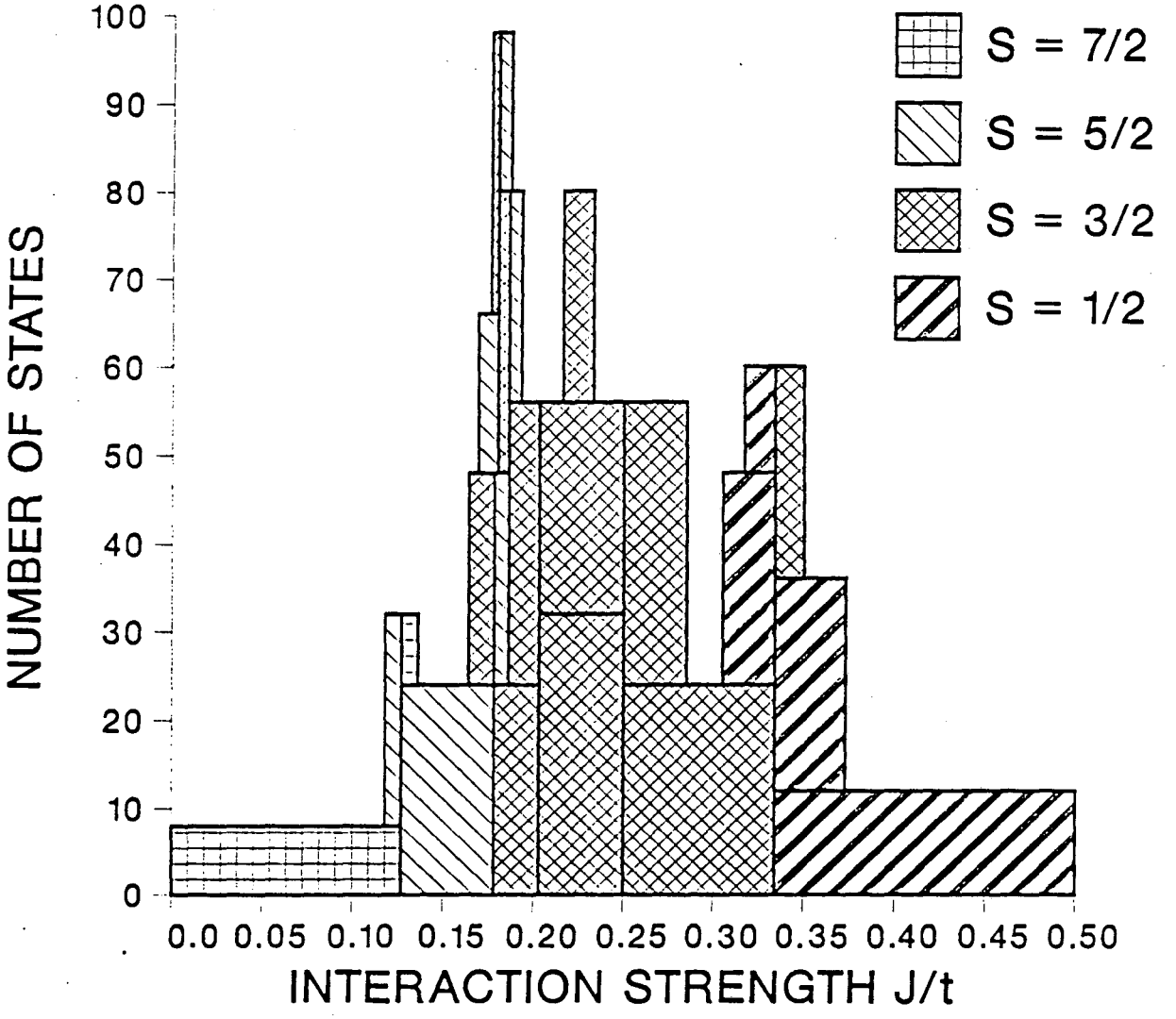
NUMBER OF STATES
100
90
80
70
60
50
40
30
20
10
0
0.0 0.05 0.10 0.15 0.20 0.25 0.30 0.35 0.40 0.45 0.50
INTERACTION STRENGTH J/t
S = 7/2
S = 5/2
S = 3/2
S = 1/2

FIGURE 12

LAWRENCE BERKELEY LABORATORY
TECHNICAL INFORMATION DEPARTMENT
1 CYCLOTRON ROAD
BERKELEY, CALIFORNIA 94720